AD NUMBER

AD922398

LIMITATION CHANGES

TO:

Approved for public release; distribution is unlimited.

FROM:

Distribution authorized to U.S. Gov't. agencies only; Test and Evaluation; SEP 1974. Other requests shall be referred to Armament Development Test Center, Eglin AFB, FL 32542.

AUTHORITY

AFATL ltr 18 Mar 1977

AEDC-TR-74-88

SEP 30 1974

AERODYNAMIC LOADS AND SEPARATION CHARACTERISTICS FROM THE F-4C AIRCRAFT FOR THE MGGB MK-II GUIDED WEAPON AT MACH NUMBERS 0.7 TO 1.3

J. B. Carman
ARO, Inc.

PROPULSION WIND TUNNEL FACILITY
ARNOLD ENGINEERING DEVELOPMENT CENTER
AIR FORCE SYSTEMS COMMAND
ARNOLD AIR FORCE STATION, TENNESSEE 37389

September 1974

Final Report for Period May 30 – June 1, 1974

Prepared for

ARMAMENT DEVELOPMENT AND TEST CENTER (SDTE)
AIR FORCE ARMAMENT LABORATORY (DLJC)
EGLIN AIR FORCE BASE, FLORIDA 32542

NOTICES

When U. S. Government drawings specifications, or other data are used for any purpose other than a definitely related Government procurement operation, the Government thereby incurs no responsibility nor any obligation whatsoever, and the fact that the Government may have formulated, furnished, or in any way supplied the said drawings, specifications, or other data, is not to be regarded by implication or otherwise, or in any manner licensing the holder or any other person or corporation, or conveying any rights or permission to manufacture, use, or sell any patented invention that may in any way be related thereto.

Qualified users may obtain copies of this report from the Defense Documentation Center.

References to named commercial products in this report are not to be considered in any sense as an endorsement of the product by the United States Air Force or the Government.

APPROVAL STATEMENT

This technical report has been reviewed and is approved.

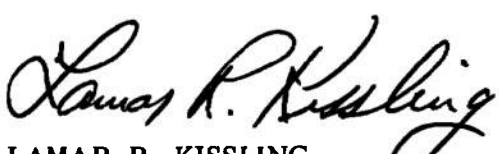

LAMAR R. KISSLING
Lt Colonel, USAF
Chief Air Force Test Director, PWT
Directorate of Test

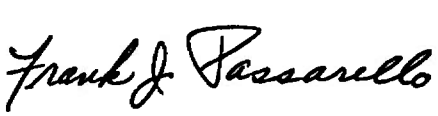

FRANK J. PASSARELLO
Colonel, USAF
Director of Test

REPORT DOCUMENTATION PAGE		READ INSTRUCTIONS BEFORE COMPLETING FORM
1. REPORT NUMBER AEDC-TR-74-88	2. GOVT ACCESSION NO.	3. RECIPIENT'S CATALOG NUMBER
4. TITLE (and Subtitle) AERODYNAMIC LOADS AND SEPARATION CHARACTERISTICS FROM THE F-4C FOR THE MGGB MK-II GUIDED WEAPON AT MACH NUMBERS 0.7 TO 1.3		5. TYPE OF REPORT & PERIOD COVERED Final Report - May 30 to June 1, 1974 6. PERFORMING ORG. REPORT NUMBER
7. AUTHOR(s) J. B. Carman - ARO, Inc.		8. CONTRACT OR GRANT NUMBER(s)
9. PERFORMING ORGANIZATION NAME AND ADDRESS Arnold Engineering Development Center (DYFS) Arnold Air Force Station Tennessee 37389		10. PROGRAM ELEMENT, PROJECT, TASK AREA & WORK UNIT NUMBERS Program Element 63741F Project 1901
11. CONTROLLING OFFICE NAME AND ADDRESS Armament Development and Test Center (SDTE) Eglin Air Force Base Florida 32542		12. REPORT DATE September 1974 13. NUMBER OF PAGES 62
14. MONITORING AGENCY NAME & ADDRESS (if different from Controlling Office)		15. SECURITY CLASS. (of this report) UNCLASSIFIED 15a. DECLASSIFICATION/DOWNGRADING SCHEDULE

16. DISTRIBUTION STATEMENT (of this Report)
Distribution limited to U.S. Government agencies only; this report contains information on test and evaluation of military hardware; September 1974; other requests for this document must be referred to Armament Development and Test Center (SDTE), Eglin Air Force Base, Florida 32542.

17. DISTRIBUTION STATEMENT (of the abstract entered in Block 20, if different from Report)

18 SUPPLEMENTARY NOTES

Available in DDC.

19 KEY WORDS (Continue on reverse side if necessary and identify by block number)

static stability
transonic flow
store separation
Modular Guided Glide Bomb (MGGB)
aerodynamic characteristics
scale model

20 ABSTRACT (Continue on reverse side if necessary and identify by block number)

Wind tunnel tests were conducted using 0.05-scale models to study the aerodynamic loads and separation characteristics from the F-4C aircraft for the MGGB MK-II store. The aerodynamic characteristics of the store were determined at free-stream conditions and at selected locations in the parent aircraft flow field. Carriage-loads data were obtained at the inboard pylon positions for aircraft angles of attack from -2 to 16 deg at parent sideslip angles of 0, 4, and 9 deg. Data were also obtained up to 20 ft away from the

20. ABSTRACT (Continued)

inboard pylons for aircraft angles of attack from 0 to 7 deg at zero sideslip. The separation trajectories were initiated from the inboard pylons for store tail fin deflection angles of 0, 20, and -20 deg at simulated altitudes of 5000 and 40,000 ft. All data were obtained at Mach numbers from 0.7 to 1.3 with the store wings in the closed position (88-deg sweep angle).

AFSC
Arnold AFS Tenn

PREFACE

The work reported herein was conducted by the Arnold Engineering Development Center (AEDC), Air Force Systems Command (AFSC), at the request of the Armament Development and Test Center (SDTE), under Program Element 63741F, Project 1901. The results were obtained by ARO, Inc. (a subsidiary of Sverdrup & Parcel and Associates, Inc.), contract operator of the AEDC, AFSC, Arnold Air Force Station, Tennessee. The work was done under ARO Project No. PA342. Data reduction was completed on June 18, 1974, and the manuscript (ARO Control No. ARO-PWT-TR-74-64), was submitted for publication on July 30, 1974.

This report is also identified as AFATL-TR-74-137 and ADTC-TR-74-77.

CONTENTS

Page

1.0 INTRODUCTION 5
2.0 APPARATUS
2.1 Test Facility 5
2.2 Test Article 6
2.3 Instrumentation 6
3.0 TEST DESCRIPTION
3.1 Test Conditions 6
3.2 Data Acquisition 7
3.3 Corrections 8
3.4 Precision of Data 8
4.0 RESULTS AND DISCUSSION
4.1 Free-Stream Aerodynamic Data 10
4.2 Aerodynamic Data in the Aircraft Flow Field 10
4.3 Separation Trajectories 11
REFERENCES 11

ILLUSTRATIONS

Figure

1. Isometric Drawing of a Typical Store Separation Installation and a Block Diagram of the Computer Control Loop 13
2. Schematic of the Tunnel Test Section Showing Model Location 14
3. Sketch of F-4C Parent-Aircraft Model 15
4. Details of the F-4 Inboard Pylon Model 15
5. Details of the F-4 370-gal Fuel Tank Model 16
6. Details of the MGGB MK-II Model 17
7. Tunnel Installation Photograph Showing Parent Aircraft, Store, and CTS 18
8. F-4C Load Configurations 19
9. Comparison of the Free-Stream Aerodynamic Characteristics of the MGGB MK-II Store for Different Fin Deflection Angles, $\beta_W = 0$ 20
10. Variation of the MGGB MK-II Longitudinal Stability Derivatives and the Pitching-Moment and Axial-Force Coefficients with Mach Number, $\alpha_B = \beta_W = 0$ 25

Figure Page

11. Variation of the Free-Stream Aerodynamic Characteristics of the MGGB MK-II Store with Sideslip Angle, $\delta_F = 0$ 26
12. Variation of the MGGB MK-II Lateral Stability Derivatives with Mach Number, $\alpha_B = \beta_W = 0$ 31
13. Aerodynamic Characteristics of the MGGB MK-II Store at the Carriage Position, $\delta_F = 0$ 32
14. Aerodynamic Characteristics of the MGGB MK-II Store in the F-4C Flow Field, $\delta_F = 0$, $X_P = Y_P = 0$, $\beta_P = 0$ 37
15. Comparison of the MGGB MK-II Launch Trajectories for Different Fin Deflection Angles, $\beta_P = 0$ 47

TABLES

1. Wind Tunnel Test Conditions 57
2. Test Summary 57
3. Full-Scale Store Parameters Used in Trajectory Calculations 58
4. Adjustments to Pitching-Moment Coefficients for Trajectory Calculations 58

NOMENCLATURE 59

1.0 INTRODUCTION

Wind tunnel store separation data for the MGGB MK-II launched from the F-4C aircraft, along with store aerodynamic characteristics in both the free-stream and parent aircraft flow field, were obtained using a six-degree-of-freedom captive trajectory store separation system (CTS). The test was conducted in the Aerodynamic Wind Tunnel (4T) of the Propulsion Wind Tunnel Facility (PWT) using 0.05-scale models of the F-4C aircraft and MGGB MK-II store. The data were obtained at Mach numbers 0.7 to 1.3 with the MGGB wings in the closed position (88-deg sweep angle). The separation trajectories were initiated from the left and right wing inboard pylons of the parent aircraft using simulated full-scale store weights, cg locations, and altitude. Other flight variables included fin deflection angle and parent aircraft angle of attack. The free-stream aerodynamic characteristics of the store were measured at angles of attack and sideslip from -20 to 20 deg. The aerodynamic coefficients in the parent flow field were measured in the plane of the left and right wing inboard pylons up to 20 ft away from the pylons for parent angles of attack from 0 to 7 deg at zero sideslip. In addition, carriage position aerodynamic data were obtained at the inboard pylons for parent aircraft angles of attack from -2 to 16 deg at sideslip angles of 0, 4, and 9 deg.

2.0 APPARATUS

2.1 TEST FACILITY

The Aerodynamic Wind Tunnel (4T) is a closed-loop, continuous-flow, variable-density tunnel in which the Mach number can be varied from 0.1 to 1.3. At all Mach numbers, the stagnation pressure can be varied from 300 to 3700 psfa. The test section is 4 ft square and 12.5 ft long with perforated, variable porosity (0.5- to 10-percent open) walls. It is completely enclosed in a plenum chamber from which the air can be evacuated, allowing part of the tunnel airflow to be removed through the perforated walls of the test section.

Two separate and independent support systems were used to support the models. The parent aircraft model was inverted in the test section and supported by an offset sting attached to the main pitch sector. The store model was supported by the CTS which extends down from the tunnel top wall and provides store movement (six degreees of freedom) independent of the parent-aircraft model. An isometric drawing of a typical installation is shown in Fig. 1.

Also shown in Fig. 1 is a block diagram of the computer control loop used during testing. The analog system and the digital computer work as an integrated unit and, utilizing required input information, control the store movement. Store positioning is accomplished

by use of six individual d-c electric motors. Maximum translational travel of the CTS is ±15 in. from the tunnel centerline in the lateral and vertical directions and 36 in. in the axial direction. Maximum angular displacements are ±45 deg in pitch and yaw and ±360 deg in roll. A more complete description of the test facility can be found in Ref. 1. A schematic showing the test section details and the location of the models in the tunnel is shown in Fig. 2.

2.2 TEST ARTICLE

The basic dimensions of the 0.05-scale F-4C parent model are presented in Fig. 3. The parent model is geometrically similar to the full-scale airplane except that the tail section is removed to minimize interference with the CTS support movement. Details of the pylons, 370-gal fuel tank and MGGB MK-II store models are shown in Figs. 4, 5, and 6, respectively. For all test phases, the store wings remained in the closed position (88-deg sweep angle) while fin deflection angles were 0, 20, and -20 deg. The ±20-deg fin deflections were obtained with a second set of fins for which all four trailing edges were physically deflected. There was no gap between the stabilizer and deflected fins. A typical tunnel installation photograph showing parent aircraft, store model, and CTS is shown in Fig. 7.

2.3 INSTRUMENTATION

A six-component internal strain-gage balance was used to obtain store aerodynamic force and moment data. Translational and angular positions of the store were obtained from CTS analog inputs during separation trajectories and from digital computer commands during aerodynamic testing. The parent-model angle of attack was determined using an internal, gravimetric angular position indicator. The pylons contained a touch wire system which enabled the store to be accurately positioned for launch. The system was also wired to automatically stop the CTS motion and give visual indication should the store or sting support make contact with any surface other than the touch wire.

3.0 TEST DESCRIPTION

3.1 TEST CONDITIONS

A complete test summary and the wind tunnel test conditions are given in Tables 1 through 4. Aerodynamic and separation trajectory data were obtained at Mach numbers from 0.7 to 1.3. Tunnel conditions were held constant at the desired Mach number, while the data were obtained. The trajectories were terminated when the store or sting contacted the parent-aircraft model or when a CTS limit was reached.

3.2 DATA ACQUISITION

3.2.1 Aerodynamic Loads Data

Store aerodynamic data in the free stream and in the parent aircraft flow field were obtained in the following manner. After tunnel conditions were established and the aircraft model angle of attack was set (when applicable), the store was manually set at α_B = 0 (free-stream data) or at the carriage position ($X_P = Y_P = Z_P = 0$, flow field data). Operational control of the CTS was then switched to the digital computer, which controlled the store movement through commands to the CTS (see block diagram, Fig. 1). The preselected orientations and cg positions of the store programmed into the computer are given in Table 2. At each position set, the wind tunnel operating conditions and the store model forces and moments were measured and recorded. The model aerodynamic loads were reduced to coefficient form and tabulated point by point using the same digital computer which controlled the CTS movement.

3.2.2 Trajectory Data

To obtain a trajectory, test conditions were established in the tunnel, and the parent model was positioned at the desired angle of attack. The store model was then oriented to a position corresponding to the store carriage location. After the store was set at the desired initial position, operational control of the CTS was switched to the digital computer which controlled the store movement during the trajectory through commands to the CTS analog system (see block diagram, Fig. 1). Data from the wind tunnel, consisting of measured model forces and moments, wind tunnel operating conditions, and CTS rig positions, were input to the digital computer for use in the full-scale trajectory calculations.

The digital computer was programmed to solve the six-degree-of-freedom equations to calculate the angular and linear displacements of the store relative to the parent aircraft pylon (Ref. 2). In general, the program involves using the last two successive measured values of each static aerodynamic coefficient to predict the magnitude of the coefficients over the next time interval of the trajectory. These predicted values are used to calculate the new position and attitude of the store at the end of the time interval. The CTS is then commanded to move the store model to this new position, and the aerodynamic loads are measured. If these new measurements agree with the predicted values, the process is continued over another time interval of the same magnitude. If the measured and predicted values do not agree within the desired precision, the calculation is repeated over a time interval one-half the previous value. This process is repeated until a complete trajectory has been obtained.

In applying the wind tunnel data to the calculations of the full-scale store trajectories, the measured forces and moments are reduced to coefficient form and then applied with proper full-scale store dimensions and flight dynamic pressure. Dynamic pressure was calculated using a flight velocity equal to the free-stream velocity component plus the components of store velocity relative to the aircraft and a density corresponding to the simulated altitude.

The initial portion of each launch trajectory incorporated simulated ejector forces in addition to the measured aerodynamic forces acting on the store. The ejector force was considered to act perpendicular to the pylon mounting surface. The ejector forces and locations along with other full-scale store parameters used in the trajectory calculations are listed in Table 3.

3.3 CORRECTIONS

Balance, sting, and support deflections caused by the aerodynamic loads on the store models were accounted for in the data reduction program to calculate the true store-model angles. Corrections were also made for model weight tares to calculate the net aerodynamic forces on the store model.

In applying the aerodynamic data from the 0.05-scale model to the calculation of full-scale missile trajectories, minor corrections in the pitching-moment coefficient data were made. Differences in the free-stream data between the present test and that reported in Ref. 3 were used to correct the 0.05-scale model data. Changes in the pitching-moment coefficient derivative (C_{m_α}) were accomplished by shifting the apparent cg of the 0.05-scale model, while the zero angle-of-attack intercept was adjusted by adding an incremental coefficient. These corrections (ΔX_{cg} and C_{m_o}) are listed in Table 4 for each Mach number at which trajectory data were obtained.

3.4 PRECISION OF DATA

Uncertainties in the basic tunnel parameters (p_t, T_t, and M_∞) were estimated from repeat calibrations of the instrumentation and from repeatability and uniformity of the test section flow during tunnel calibration. These uncertainties were then used to estimate the uncertainties in other free-stream properties, using the Taylor Series method of error propagation (Ref. 4).

	Uncertainty, percent					
Free-Stream Mach Number	M_∞	p_t	T_t	q_∞	p_∞	Re_∞
0.70	±0.3	±0.1	±0.4	±0.4	±0.2	±0.6
0.90	±0.3	±0.1	±0.4	±0.3	±0.3	±0.5

Free-Stream Mach Number	Uncertainty, percent					
	M_∞	p_t	T_t	q_∞	p_∞	Re_∞
0.95	±0.3	±0.1	±0.4	±0.3	±0.4	±0.5
1.10	±0.6	±0.1	±0.4	±0.4	±0.8	±0.5
1.30	±1.1	±0.1	±0.4	±0.3	±2.0	±0.5

The balance uncertainties, based on a 95-percent confidence level, were combined with the uncertainties in the tunnel parameters, assuming a Taylor series error propagation, to estimate the precision of the aerodynamic coefficients. The maximum estimated uncertainties are given as follow:

Free-Stream Mach Number	Uncertainty					
	C_N	C_m	C_Y	C_n	C_ℓ	C_A
0.70	±0.005	±0.004	±0.003	±0.003	±0.002	±0.002
0.90	±0.004	±0.003	±0.003	±0.003	±0.001	±0.002
0.95	±0.004	±0.003	±0.003	±0.003	±0.001	±0.002
1.10	±0.004	±0.004	±0.003	±0.002	±0.001	±0.002
1.30	±0.003	±0.003	±0.002	±0.002	±0.001	±0.001

The estimated uncertainties in store model positioning from the ability of the CTS to set on a specified value were ±0.08 ft full-scale equivalent in X, Y, and Z, ±0.15 deg in pitch and yaw, and ±1.0 deg in roll. The estimated uncertainties in parent-aircraft angles of attack and sideslip are ±0.1 and ±0.2 deg, respectively.

The trajectory data are subject to error from several sources including tunnel conditions, balance measurements, extrapolation tolerances allowed in the predicted coefficients, computer inputs, and CTS positioning control. Extrapolation tolerances were ±0.10 for the aerodynamic coefficients. The maximum uncertainties in the full-scale position data caused by the balance inaccuracies are given below:

Free-Stream Mach Number	Uncertainty					
	t, sec	X, ft	Y, ft	Z, ft	θ, deg	ψ, deg
0.70	0.4	±0.1	±0.1	±0.1	±0.4	±0.4
0.90	↓	↓	↓	↓	±0.1	±0.1
0.95	↓	↓	↓	↓	±0.5	±0.5
1.30	↓	↓	↓	↓	±0.2	±0.2

4.0 RESULTS AND DISCUSSION

Data obtained during the test consisted of MK-84 MGGB MK-II aerodynamic data in the free stream and in the F-4C flow field, along with separation trajectories of the store launched from the inboard wing pylons of the F-4C. Summaries of the test conditions and data obtained are given in Tables 1 and 2, while the aircraft load configurations are identified in Fig. 8.

4.1 FREE-STREAM AERODYNAMIC DATA

The store free-stream aerodynamic characteristics are presented in Figs. 9 through 12. Deflection of the tail fins produced incremental changes in C_N, C_m, and C_A at angles of attack from -20 to 20 deg, but little effect was noted on C_Y, C_n, and C_ℓ (Fig. 9). The 0.05-scale model longitudinal stability and axial-force characteristics at $\alpha_B = 0$ are compared with the Ref. 3 data (0.20-scale model) in Fig. 10. No notable differences in the normal-force derivatives or axial-force coefficients were evident for the two different-scale models. The small differences in the pitching-moment coefficients and derivatives for the two models can probably be attributed to the inability to accurately reproduce the true external shape at such a small scale (e.g., fin leading edges and profile). For the variation of the lateral coefficients with sideslip angle (Fig. 11), only C_ℓ seemed to be appreciably affected by the ±5 deg changes in angle of attack. Similarly, comparison of the lateral stability derivatives for the 0.05- and 0.20-scale models (Fig. 12) showed measurable differences only in C_{ℓ_β}.

4.2 AERODYNAMIC DATA IN THE AIRCRAFT FLOW FIELD

The store aerodynamic characteristics in the F-4C flow field are shown in Figs. 13 and 14. The carriage loads data (Fig. 13) show that variations in the parent aircraft angle of attack or sideslip influenced all the coefficients. These coefficient changes can be attributed primarily to changes in cross flow beneath the wings with changes in aircraft orientation. It should be noted that the data on the aircraft left wing at positive aircraft sideslip angles can be made equivalent to negative aircraft sideslip angles on the right wing by reversing the signs of C_Y, C_n, and C_ℓ (Fig. 13e). The variations of the store aerodynamic coefficients with varying distances from the pylons are shown in Fig. 14. These data indicated that the flow-field influence on store aerodynamics extended several feet away from the parent aircraft and became more pronounced as angle of attack of the parent was increased. Also, flow-field effects were evident at greater distances from the parent aircraft as free-stream Mach number was increased.

4.3 SEPARATION TRAJECTORIES

All trajectories obtained were for use in the determination of safe separation envelopes. No attempt will be made in this report to establish these envelopes or to qualify the store as safe or unsafe for aircraft separation. The trajectory data are presented as obtained from the wind tunnel along with comments regarding the aerodynamics of the store in the aircraft flow field.

The ejector-separated trajectories simulated release from the right and left wing inboard pylons. Data showing the linear displacements of the store relative to the carriage position and the angular displacements relative to the flight-axis system are presented as functions of full-scale trajectory time. Positive X, Y, and Z displacements (as seen by the pilot) are forward, to the right and down, respectively. Positive changes in θ and ψ (as seen by the pilot) are nose up and nose to the right, respectively. The model was not allowed to roll during all trajectories. Table 3 lists the full-scale store parameters used in the trajectory calculations, and the pitching-moment corrections (see Section 3.3) applied to the store model data are given in Table 4.

Launch trajectories for the MGGB MK-II are presented in Fig. 15. At δ_F = 0, the store pitched down gradually, seeking its trim condition at a small negative angle of attack (as supported by the free-stream data). Deflection of the tail fins caused the store to sharply pitch down (δ_F = 20 deg) or pitch up (δ_F = -20 deg) as would be expected. Also, there was no tendency for the store with deflected fins to recover in pitch during the time period of these trajectories. By comparison, fin deflection effects on the other trajectory parameters were minor.

REFERENCES

1. Test Facilities Handbook (Tenth Edition). "Propulsion Wind Tunnel Facility, Vol. 4." Arnold Engineering Development Center, May 1974.

2. Christopher, J. P. and Carleton, W. E. "Captive-Trajectory Store-Sepration System of the AEDC-PWT 4-Foot Transonic Tunnel." AEDC-TR-68-200 (AD839743), September 1968.

3. Webb, J. A. "Static Stability and Control Effectiveness of the MK-84 Modular Guided Glide Bomb II at Transonic Mach Numbers." AEDC-TR-74-58 (AD920703L), July 1974.

4. Beers, Yardley. Introduction to the Theory of Error. Addison-Wesley Publishing Company, Inc., Reading, Massachusetts, 1957, pp. 26-36.

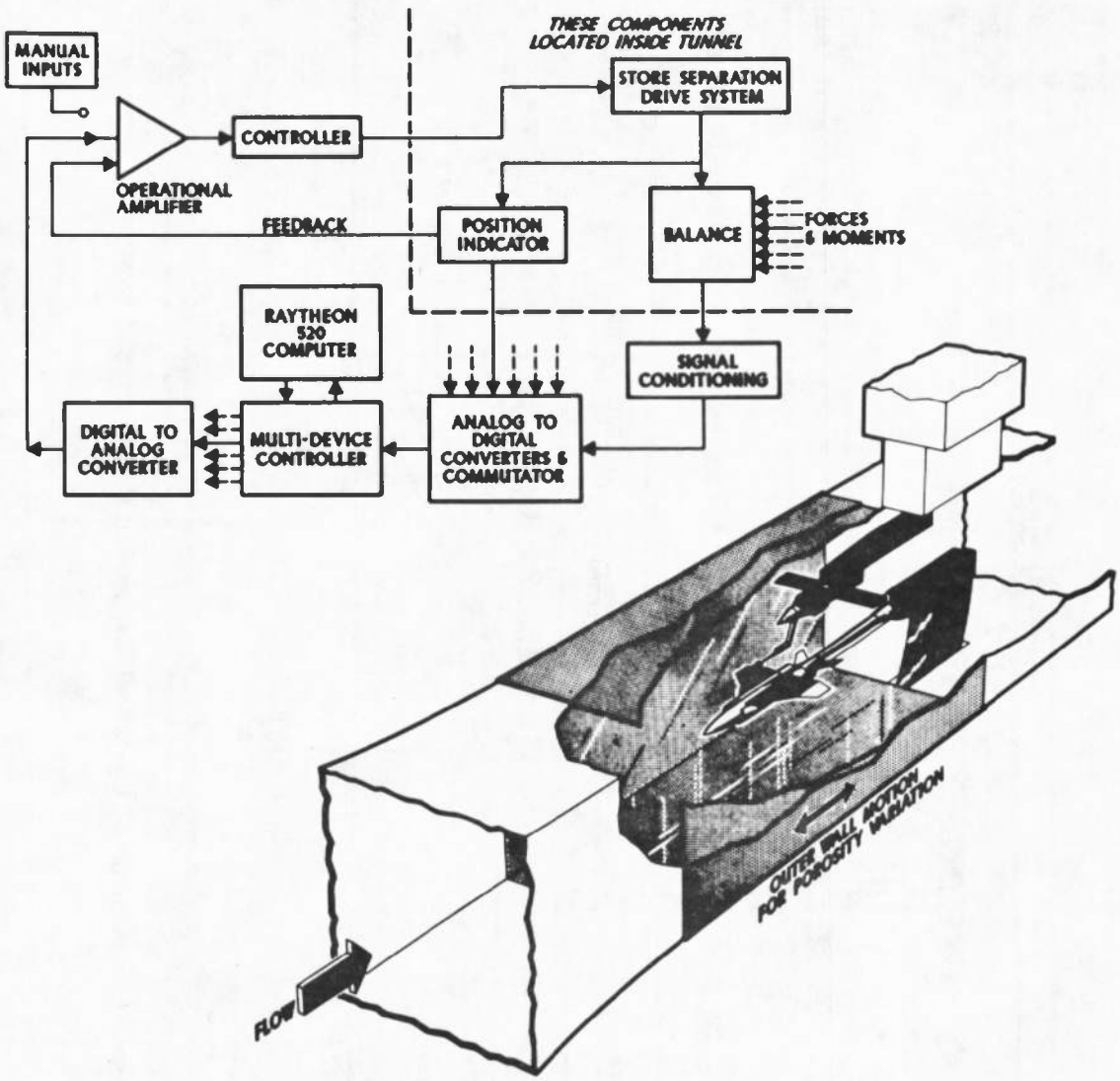

Figure 1. Isometric drawing of a typical store separation installation and a block diagram of the computer control loop.

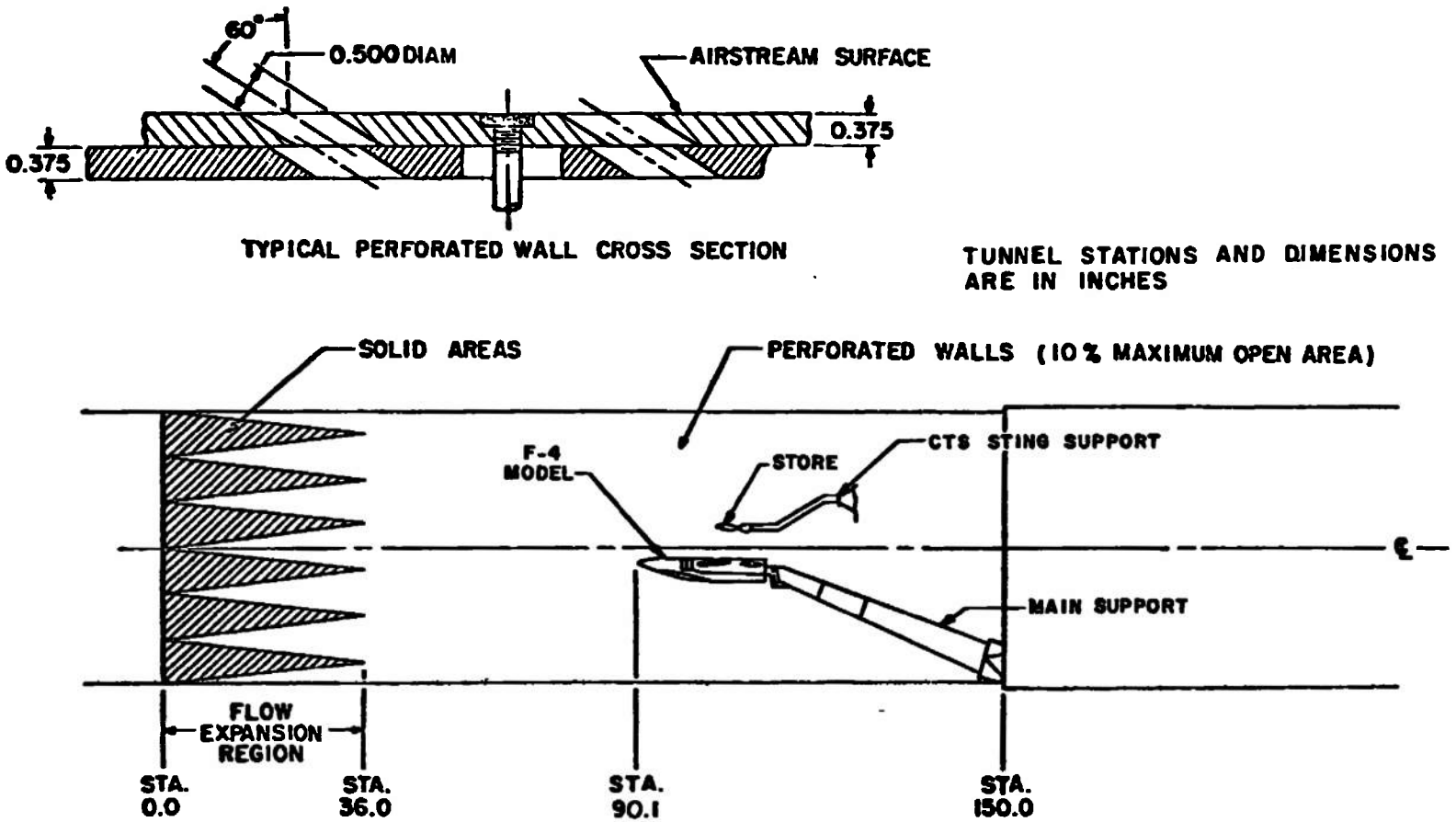

Figure 2. Schematic of the tunnel test section showing model location.

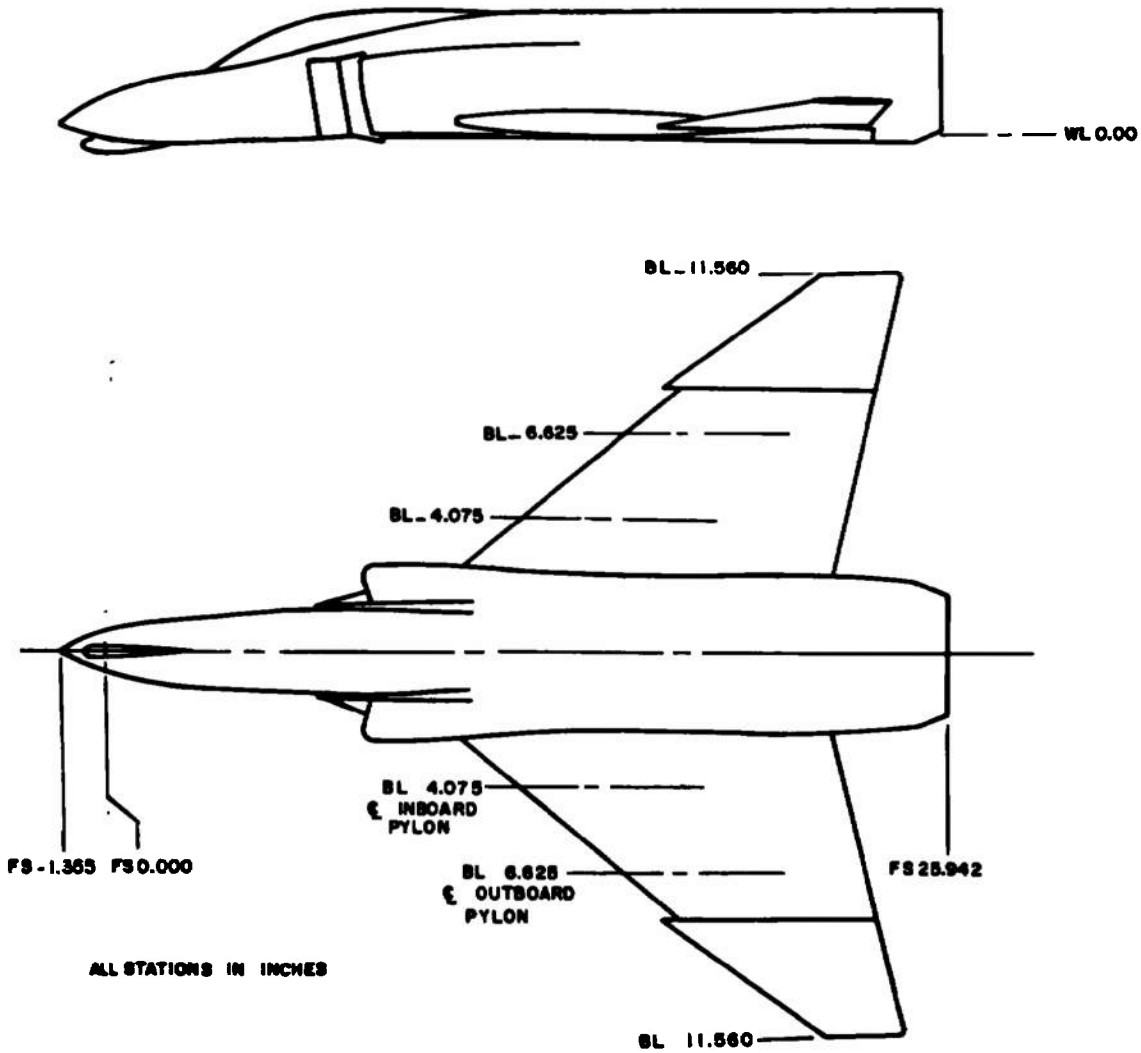

Figure 3. Sketch of F-4C parent-aircraft model.

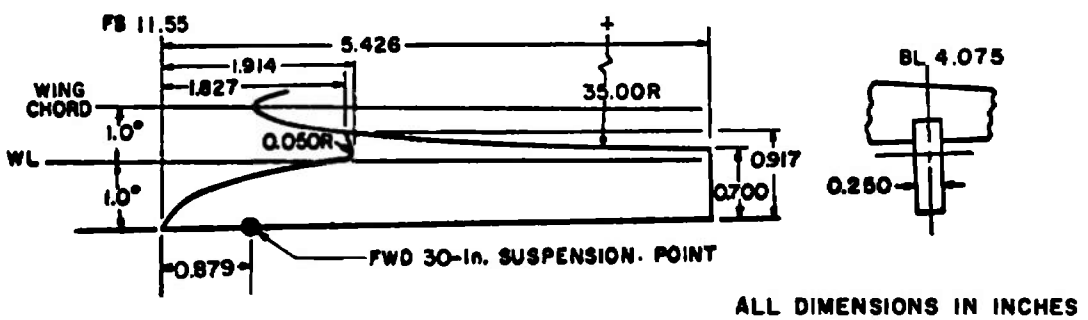

Figure 4. Details of the F-4 inboard pylon model.

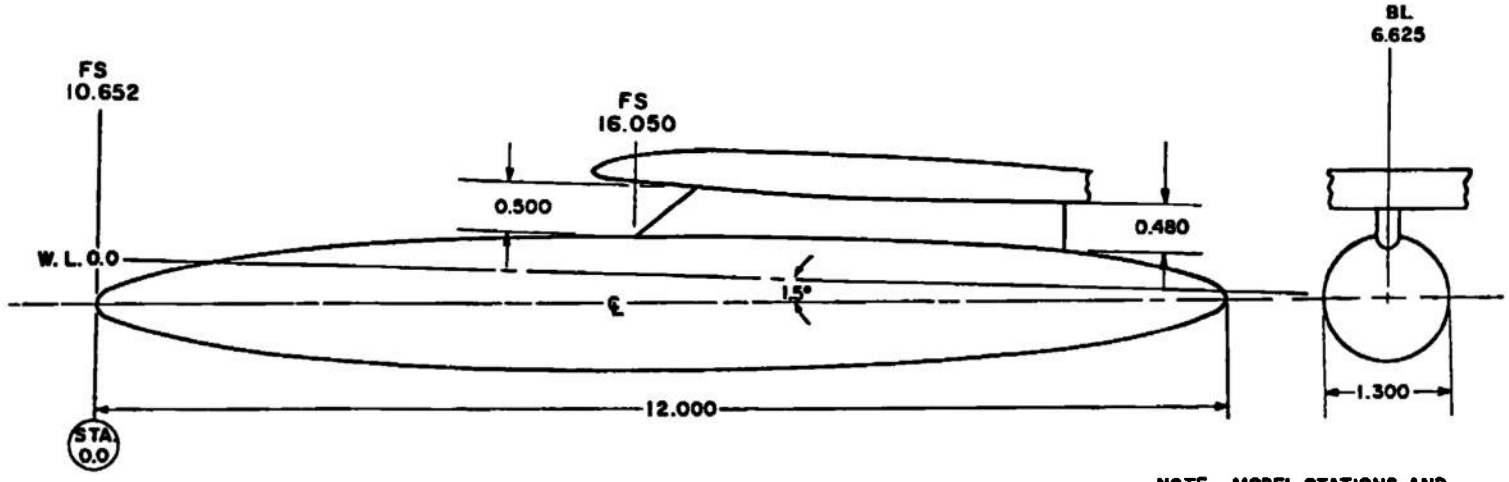

NOTE: MODEL STATIONS AND DIMENSIONS IN INCHES

BODY CONTOUR, TYPICAL BOTH ENDS

STATION	BODY DIAM	STATION	BODY DIAM
0.000	0.000	2.500	1.116
0.025	0.100	2.750	1.156
0.050	0.144	3.000	1.190
0.150	0.258	3.250	1.218
0.250	0.340	3.500	1.242
0.500	0.498	3.750	1.260
0.750	0.622	4.000	1.274
1.000	0.724	4.250	1.286
1.250	0.812	4.500	1.294
1.500	0.890	4.750	1.298
1.750	0.958	5.000	1.300
2.000	1.016	6.000	1.300
2.250	1.070		

Figure 5. Details of the F-4 370-gal fuel tank model.

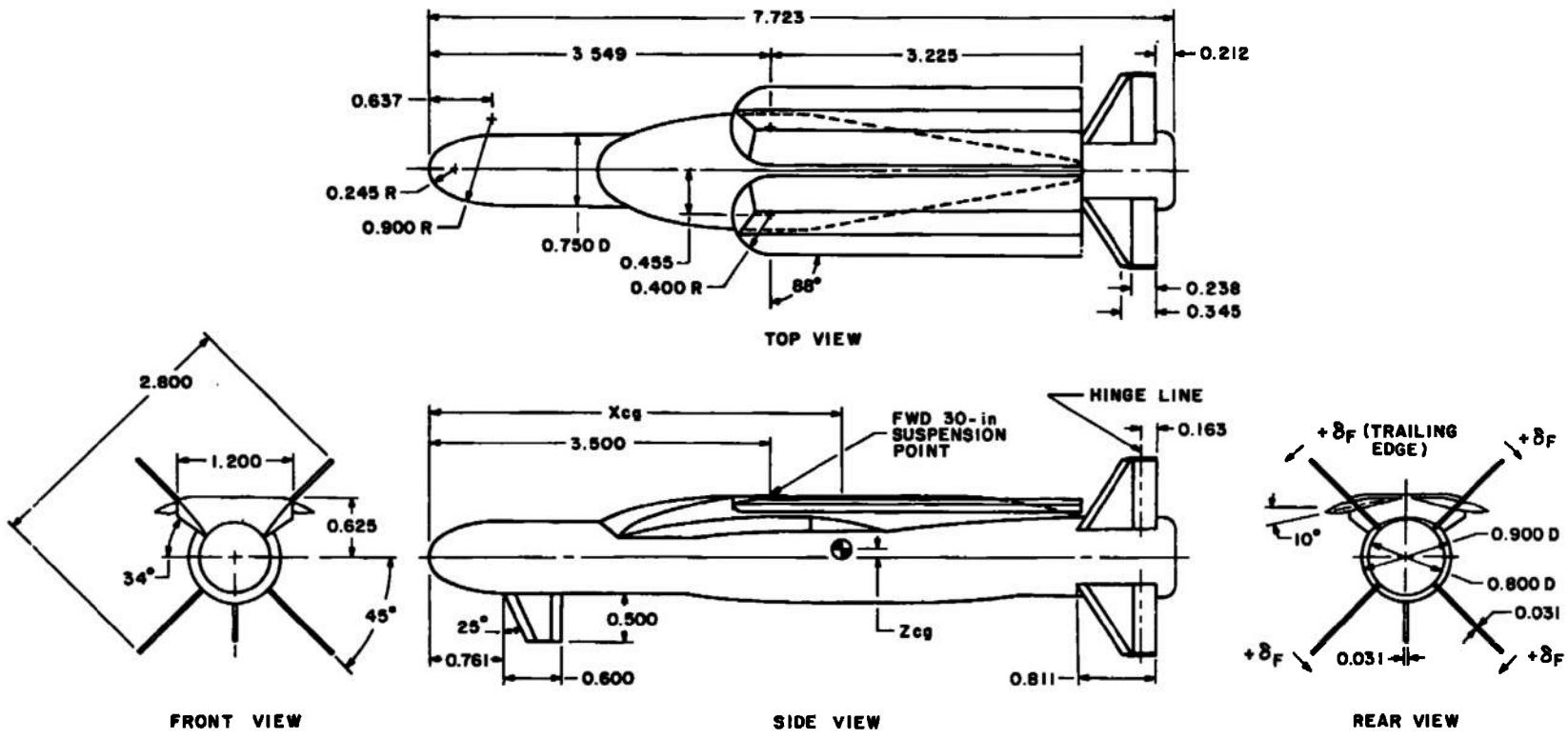

Figure 6. Details of the MGGB MK-II model.

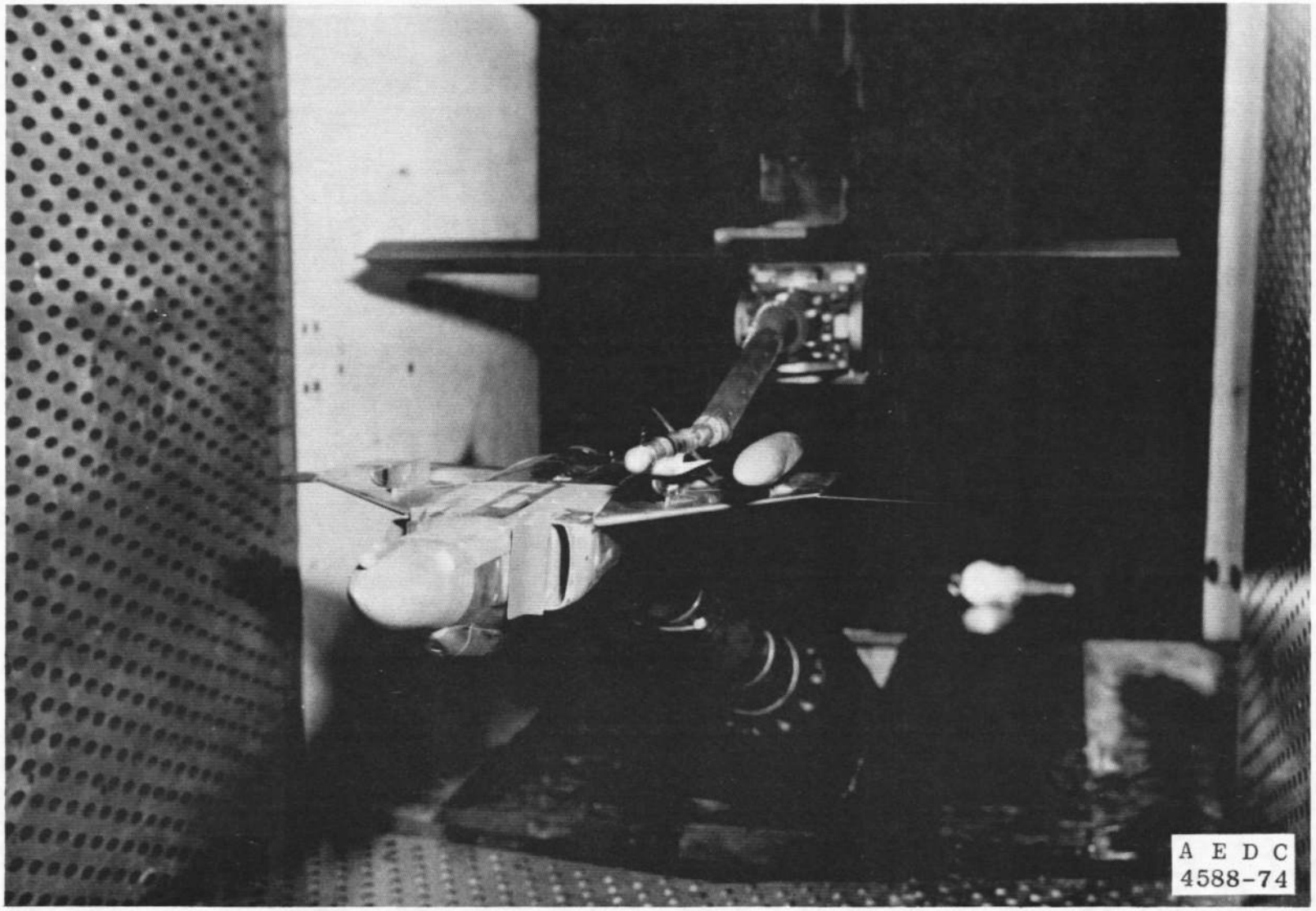

Figure 7. Tunnel installation photograph showing parent aircraft, store, and CTS.

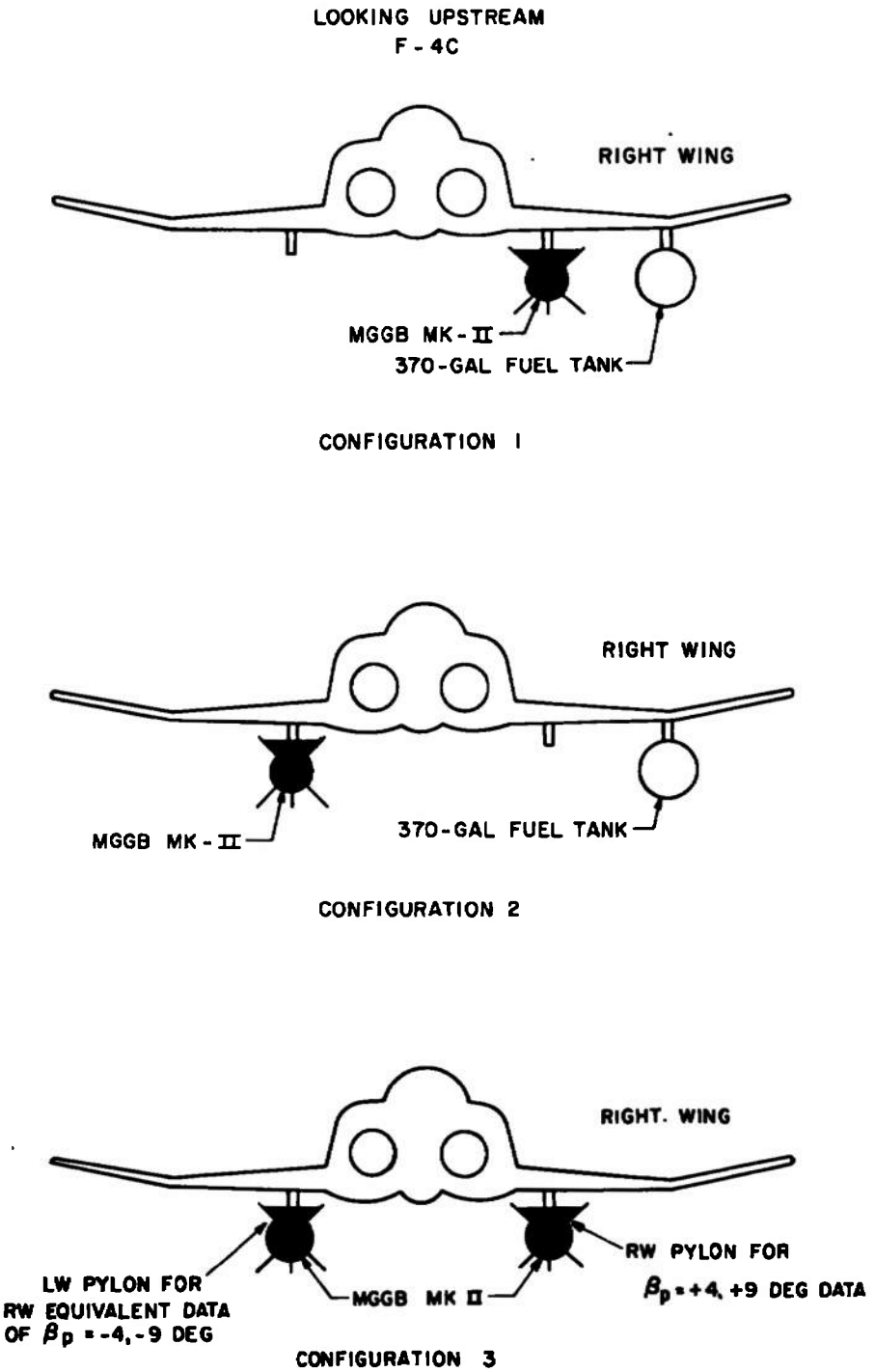

Figure 8. F-4C load configurations.

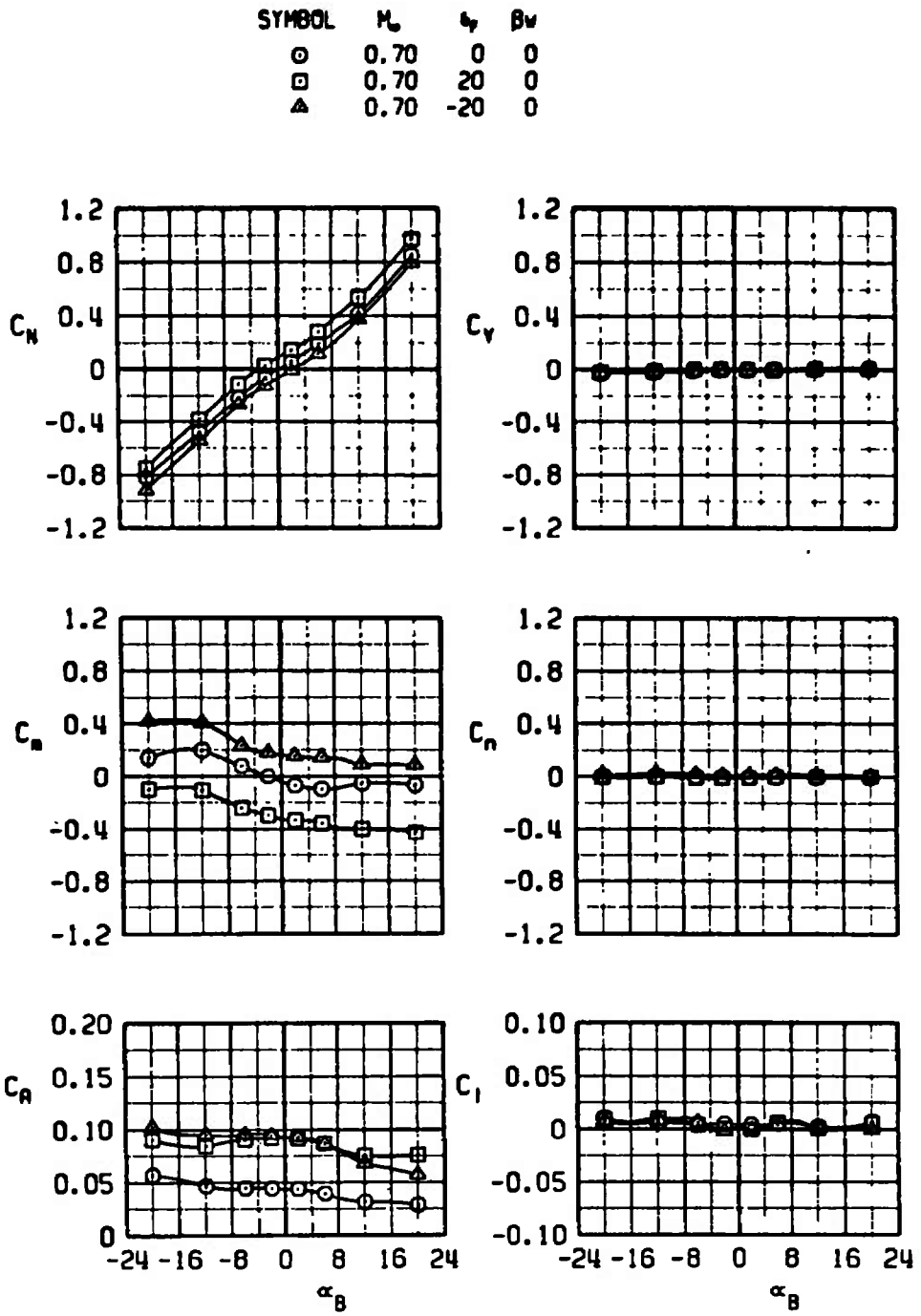

a. $M_\infty = 0.70$

Figure 9. Comparison of the free-stream aerodynamic characteristics of the MGGB MK-II store for different fin deflection angles, $\beta_W = 0$.

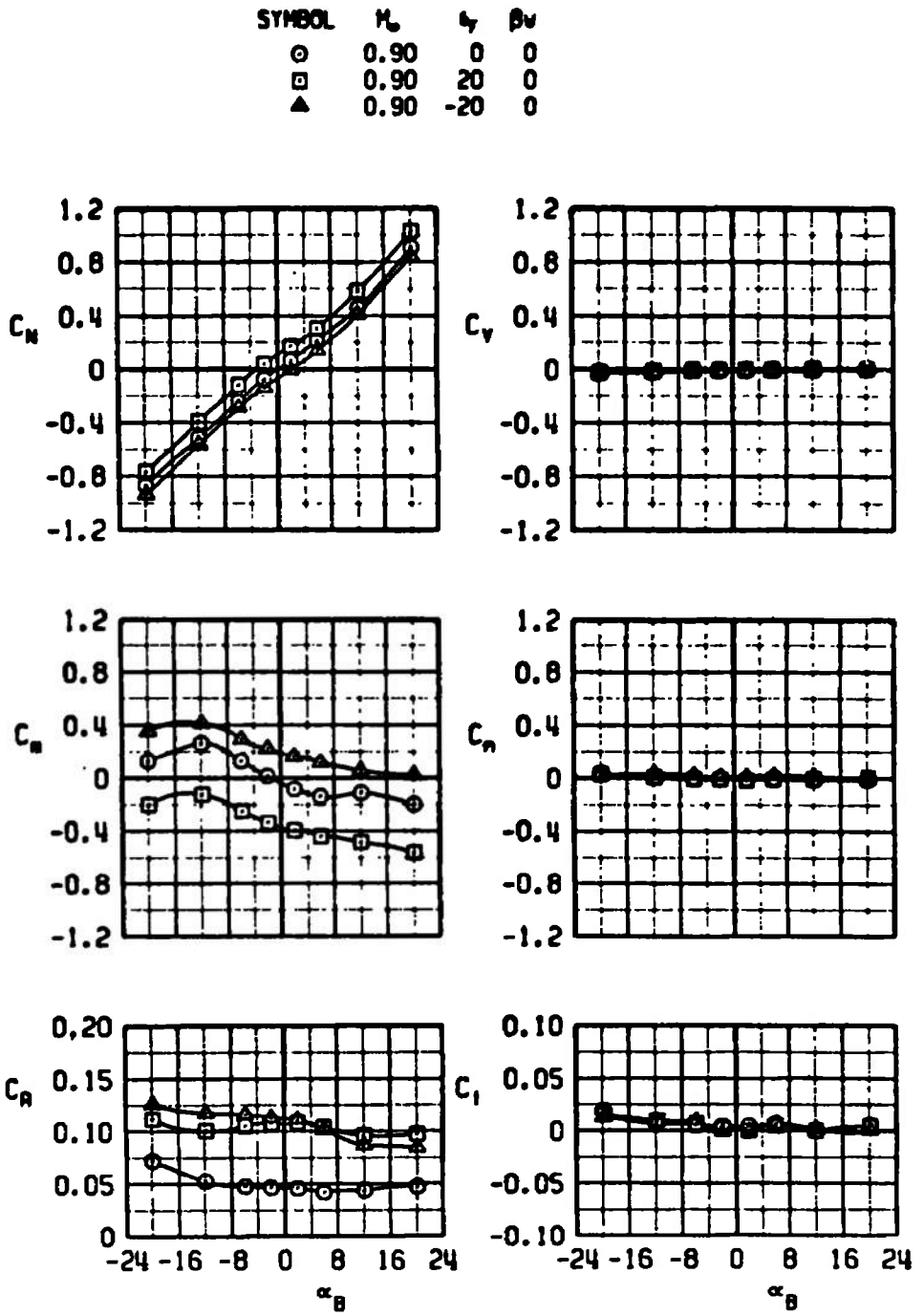

b. $M_\infty = 0.90$

Figure 9. Continued.

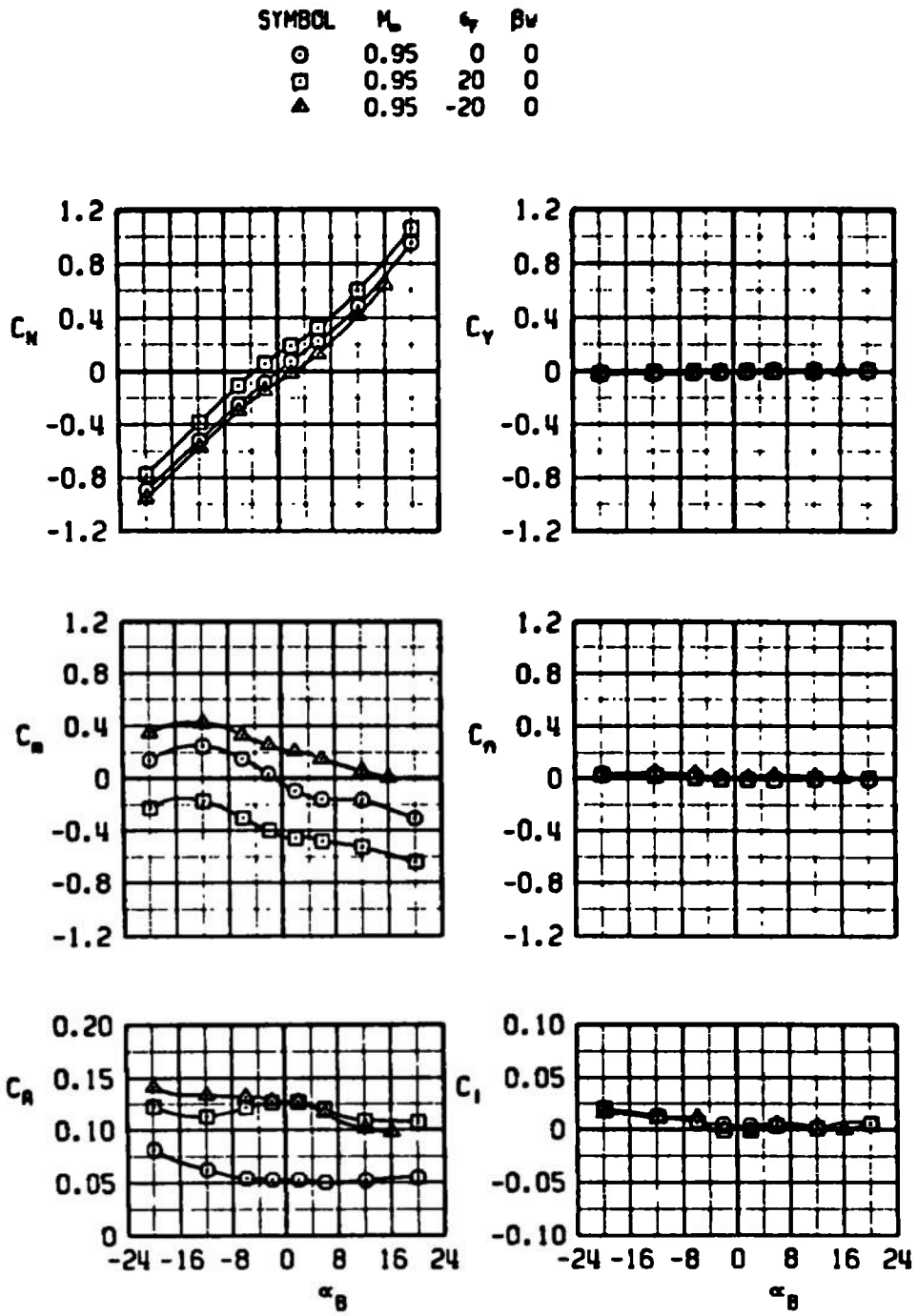

c. $M_\infty = 0.95$

Figure 9. Continued.

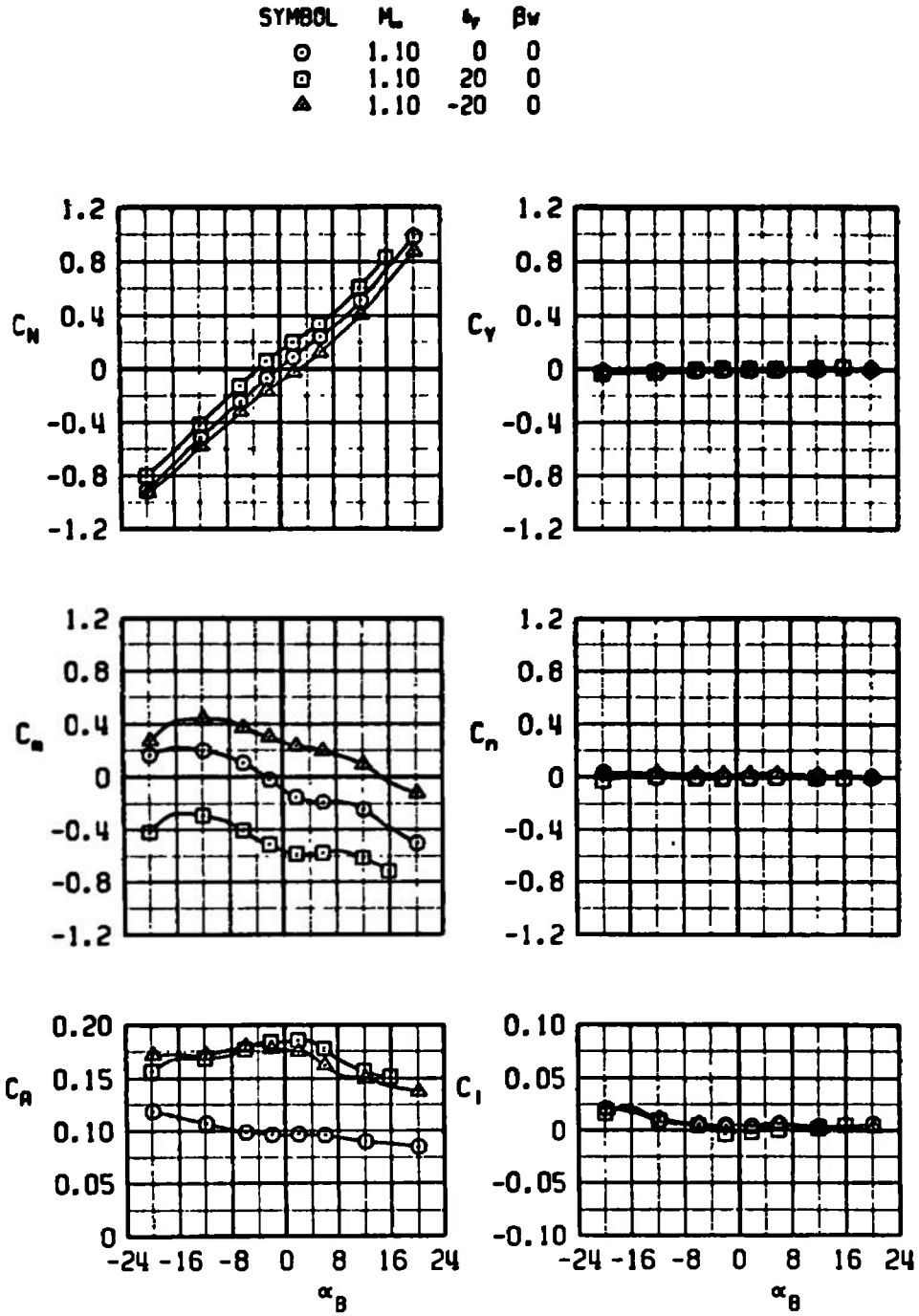

d. $M_\infty = 1.10$

Figure 9. Continued.

SYMBOL	M_∞	ϕ_v	β_v
⊙	1.30	0	0
⊡	1.30	20	0
▲	1.30	-20	0

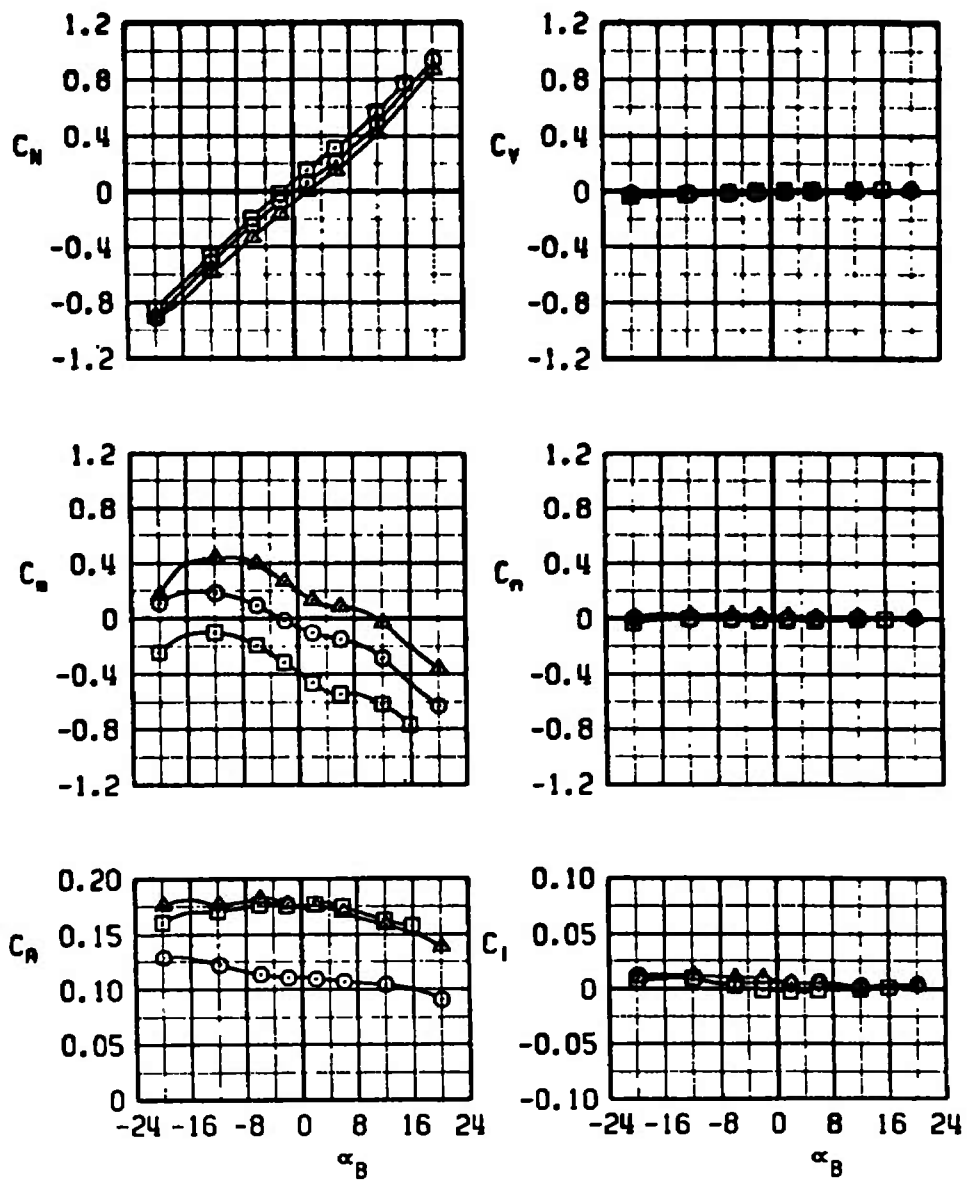

e. $M_\infty = 1.30$

Figure 9. Concluded.

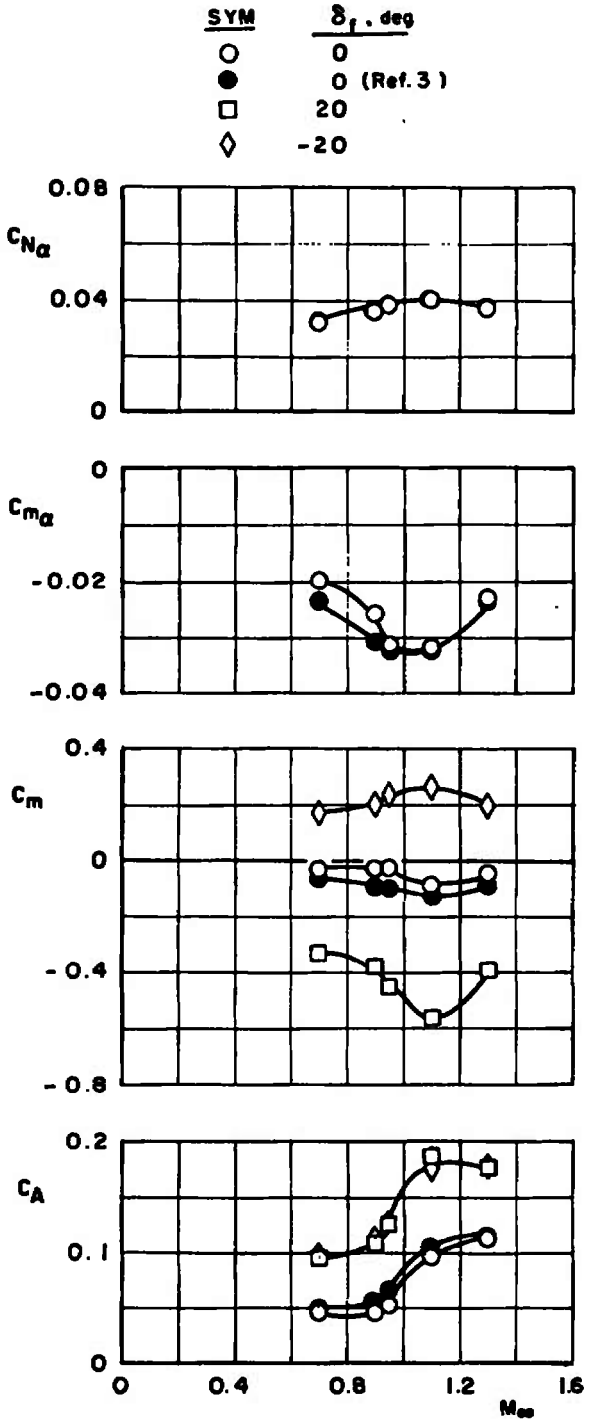

Figure 10. Variation of the MGGB MK-II longitudinal stability derivatives and the pitching-moment and axial-force coefficients with Mach number, $\alpha_B = \beta_W = 0$.

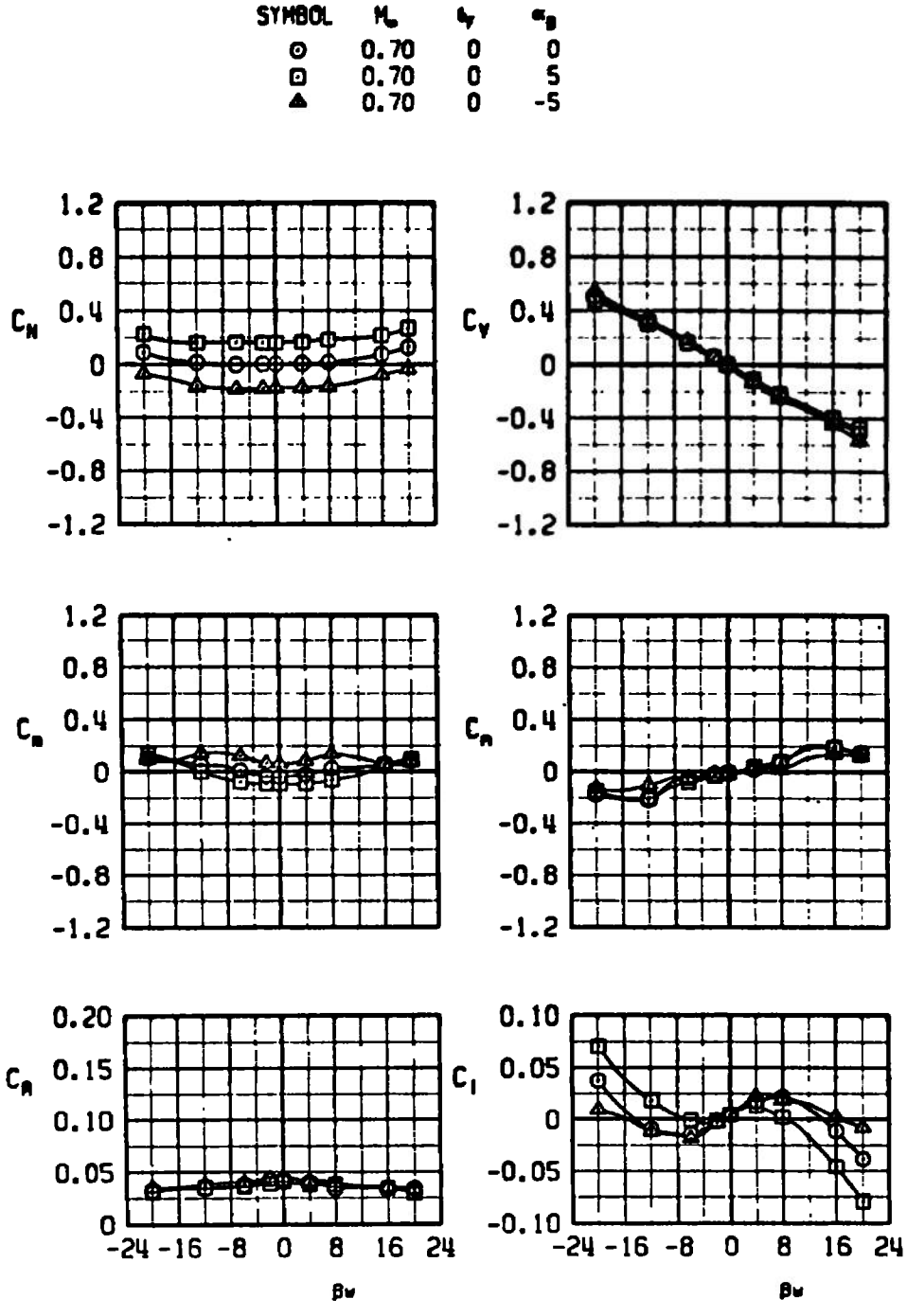

a. $M_\infty = 0.70$

Figure 11. Variation of the free-stream aerodynamic characteristics of the MGGB MK-II store with sideslip angle, $\delta_F = 0$.

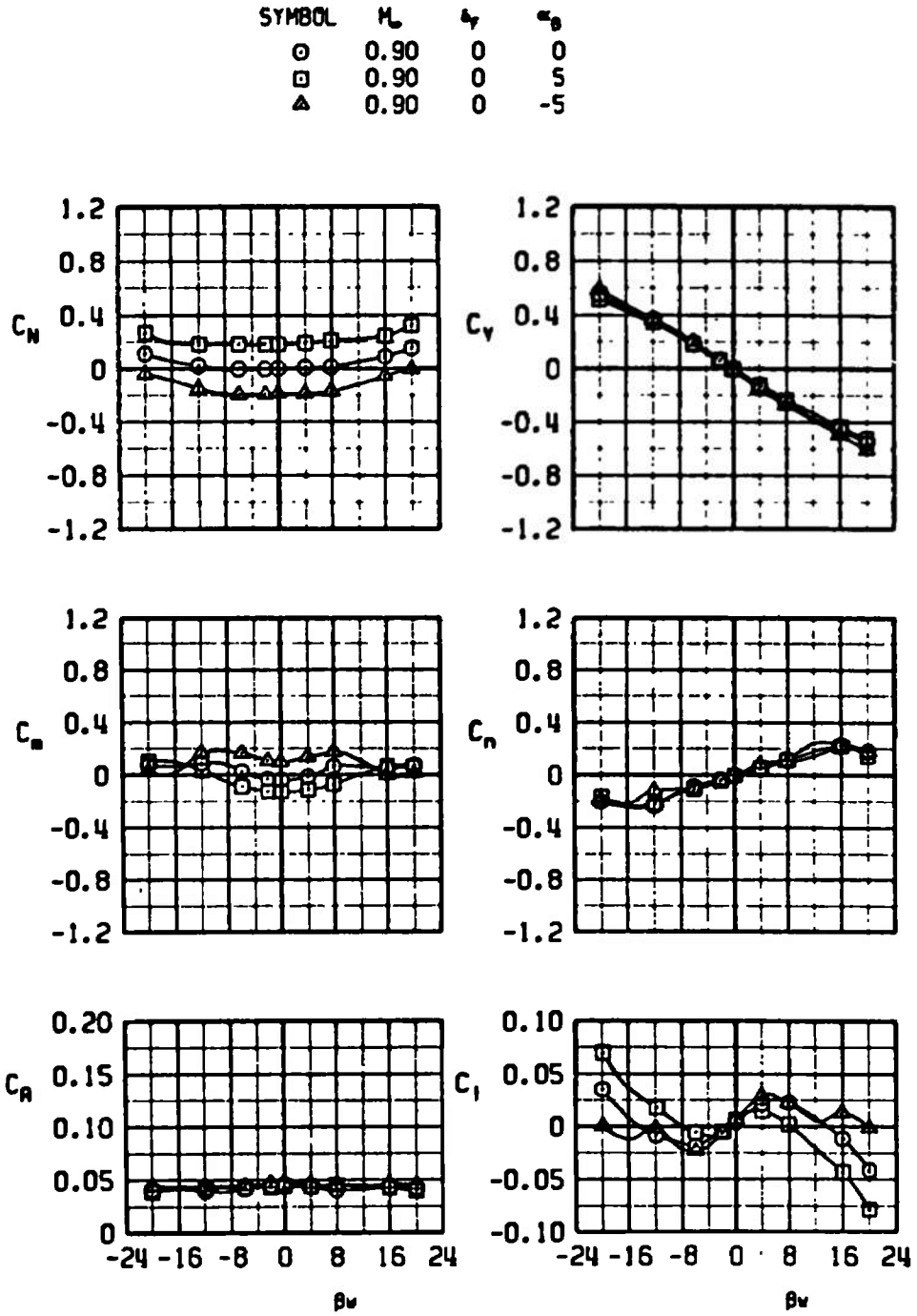

b. $M_\infty = 0.90$

Figure 11. Continued.

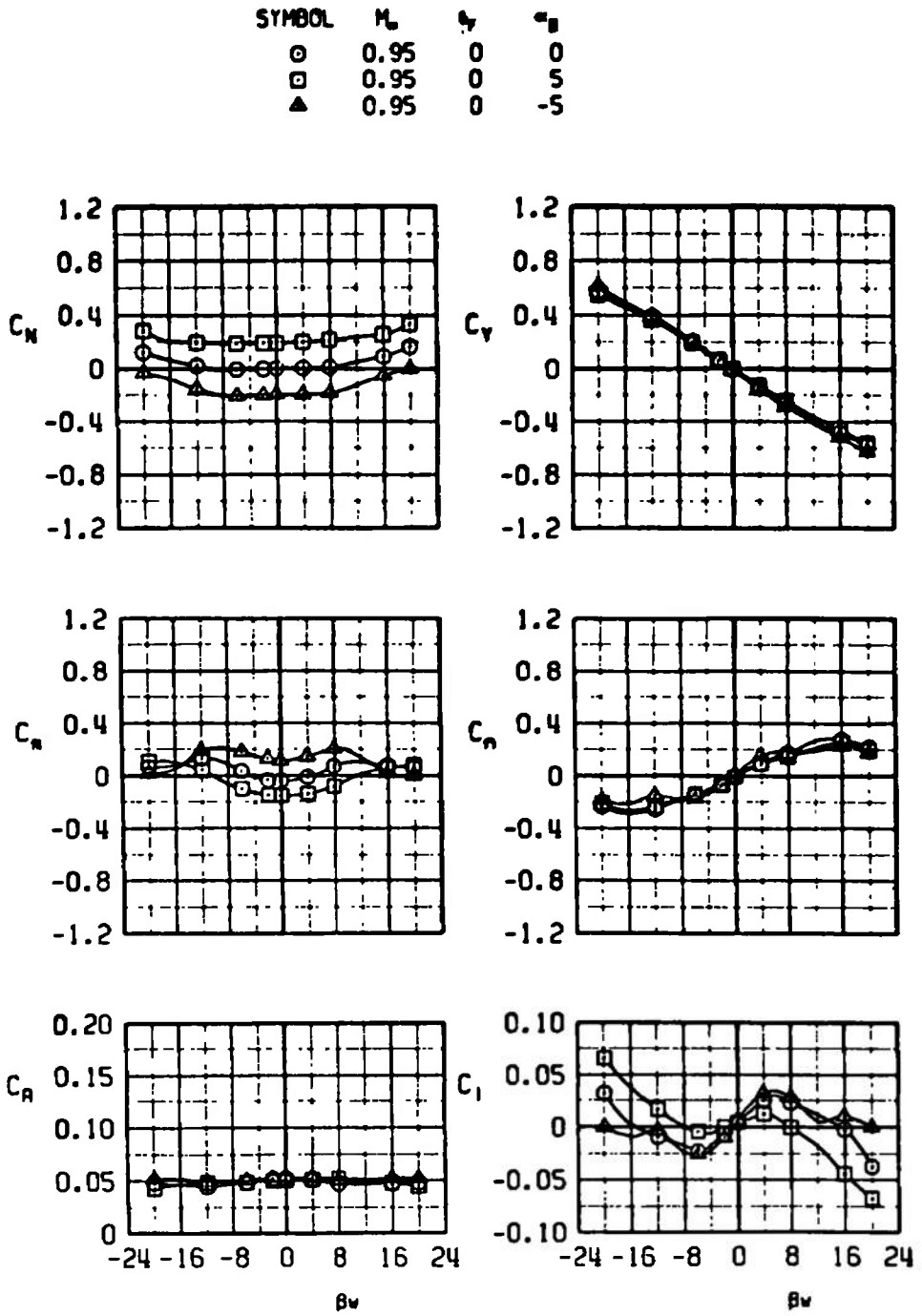

c. $M_\infty = 0.95$

Figure 11. Continued.

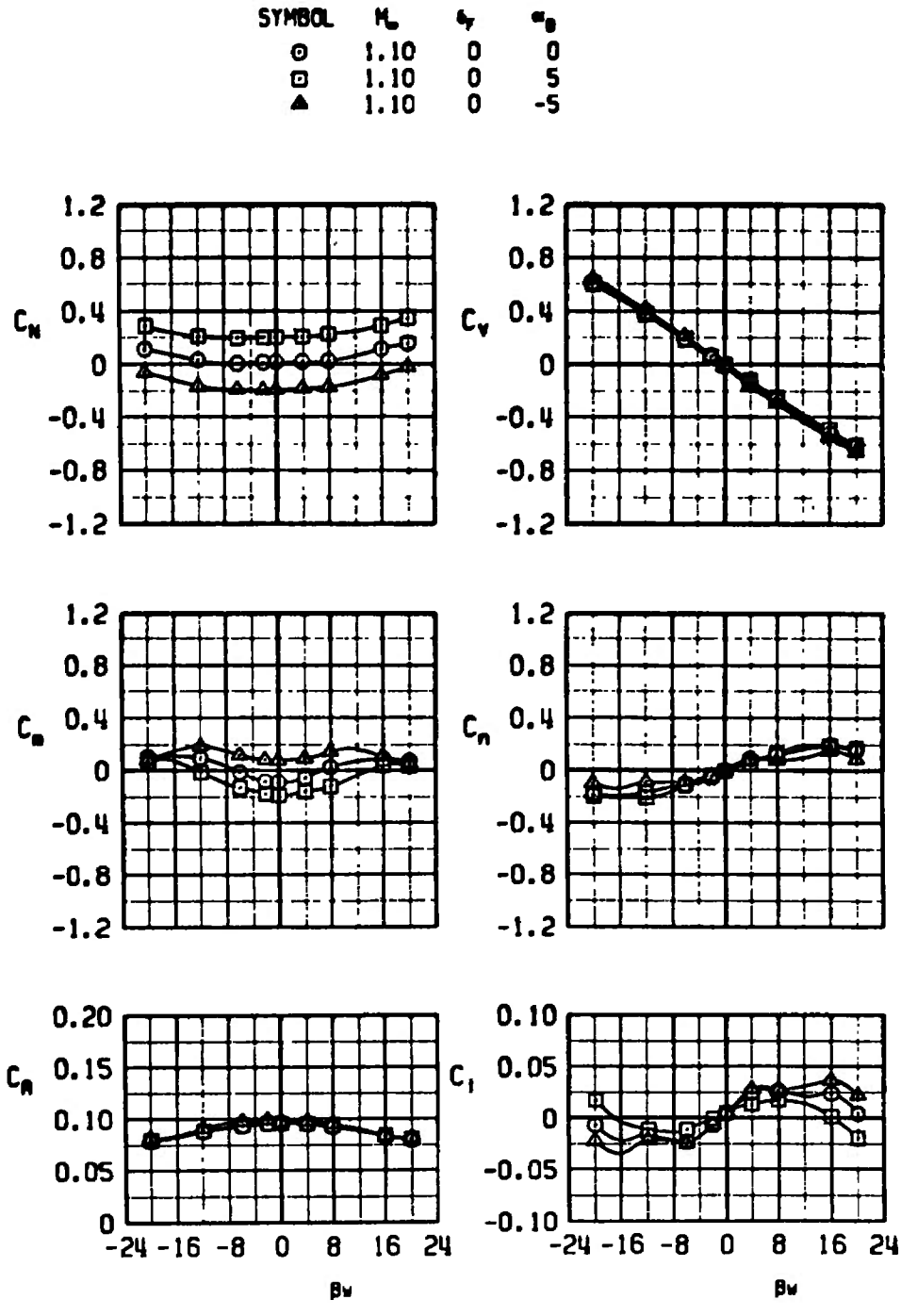

d. $M_\infty = 1.10$

Figure 11. Continued.

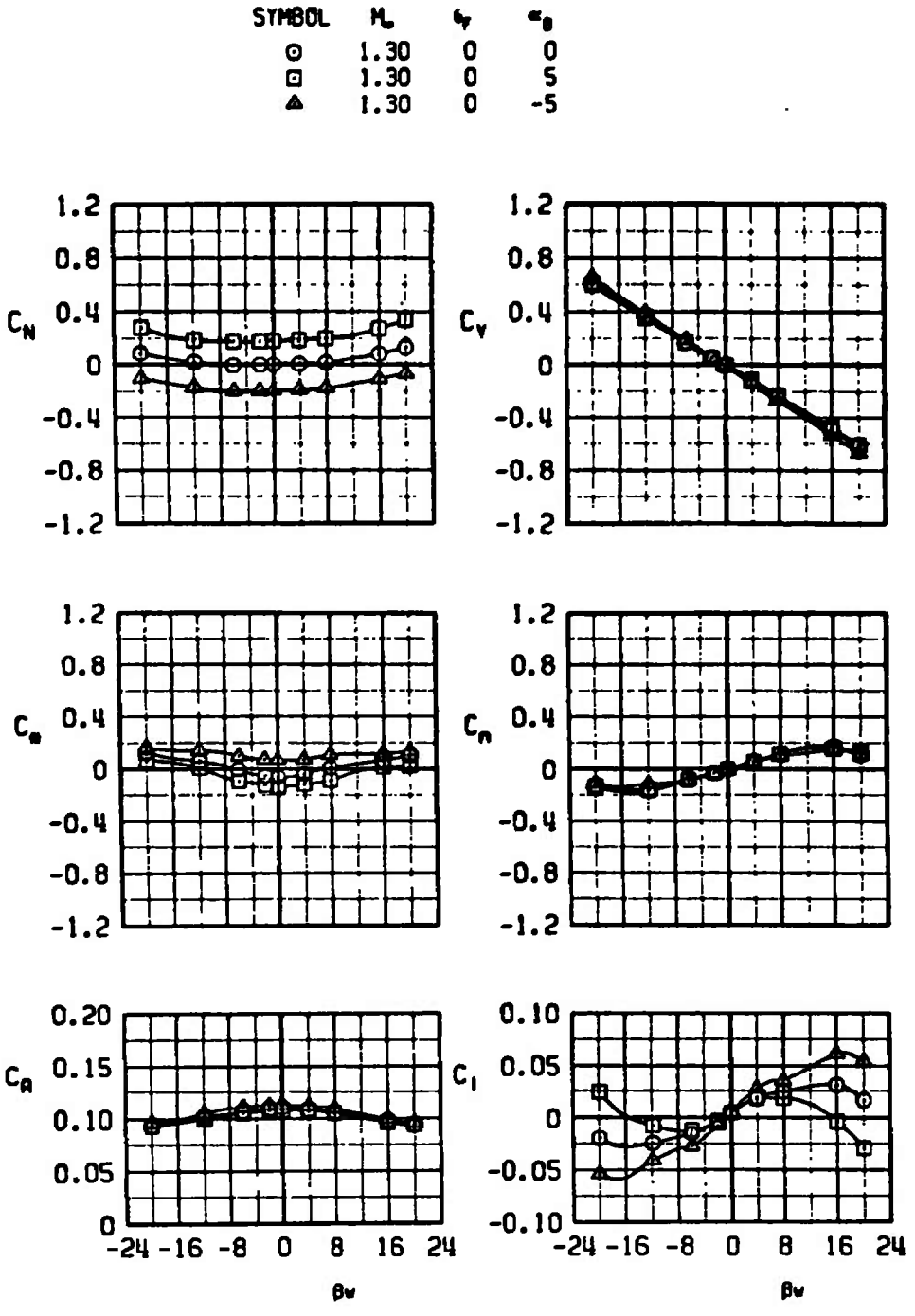

e. $M_\infty = 1.30$

Figure 11. Concluded.

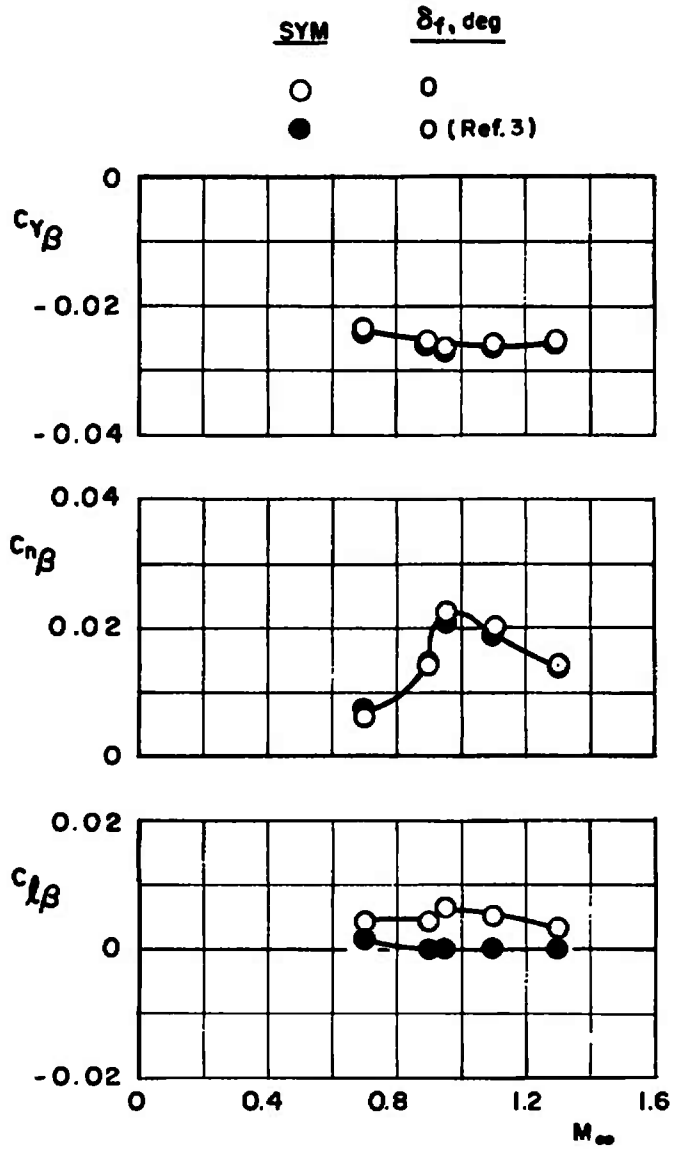

Figure 12. Variation of the MGGB MK-II lateral stability derivatives with Mach number, $\alpha_B = \beta_W = 0$.

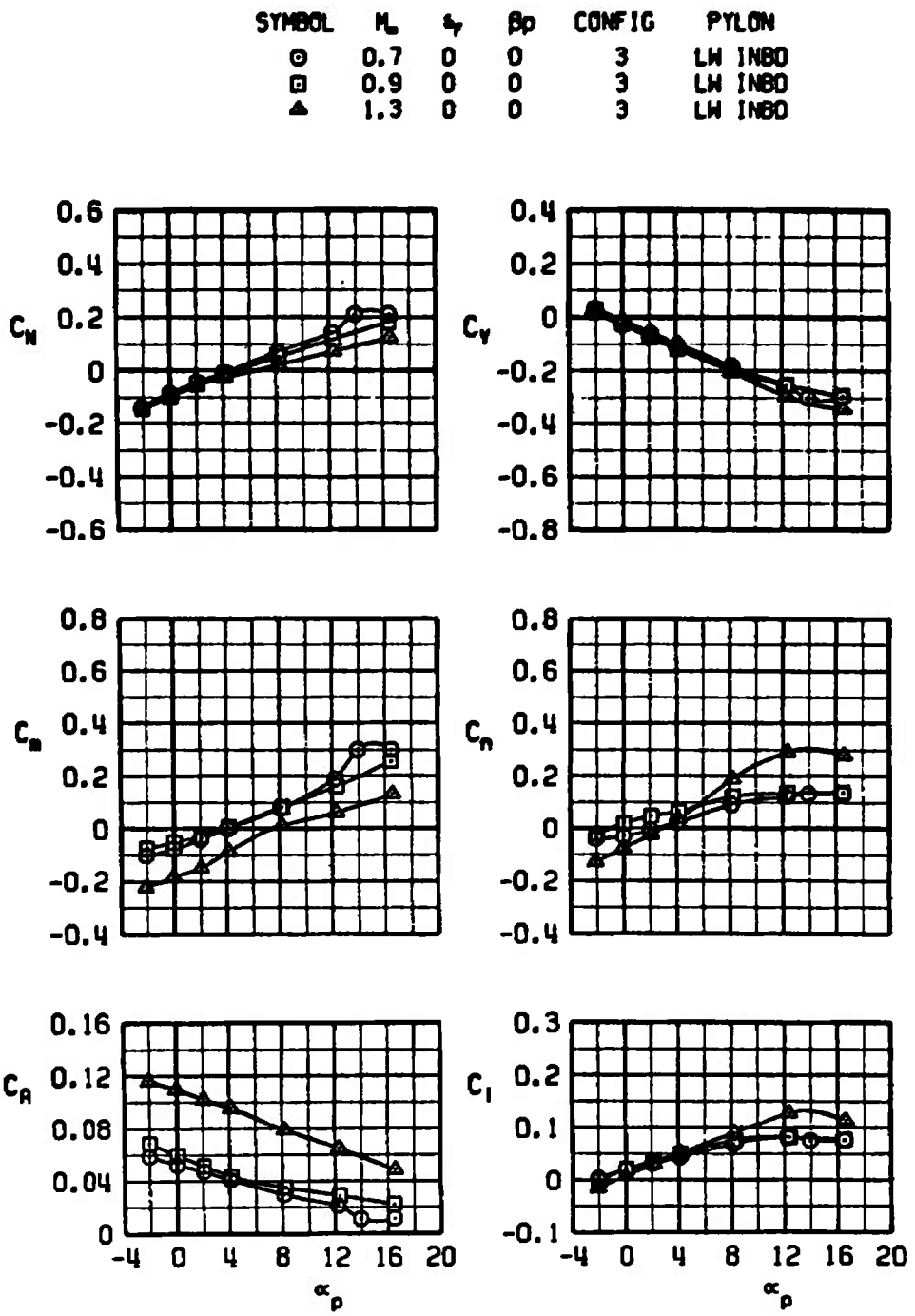

a. Variation with α_p, LW inboard, $\beta_p = 0$

Figure 13. Aerodynamic characteristics of the MGGB MK-II store at the carriage position, $\delta_F = 0$.

SYMBOL	M_∞	ϕ_T	β_p	CONFIG	PYLON
▲	1.3	0	4	3	RW INBD

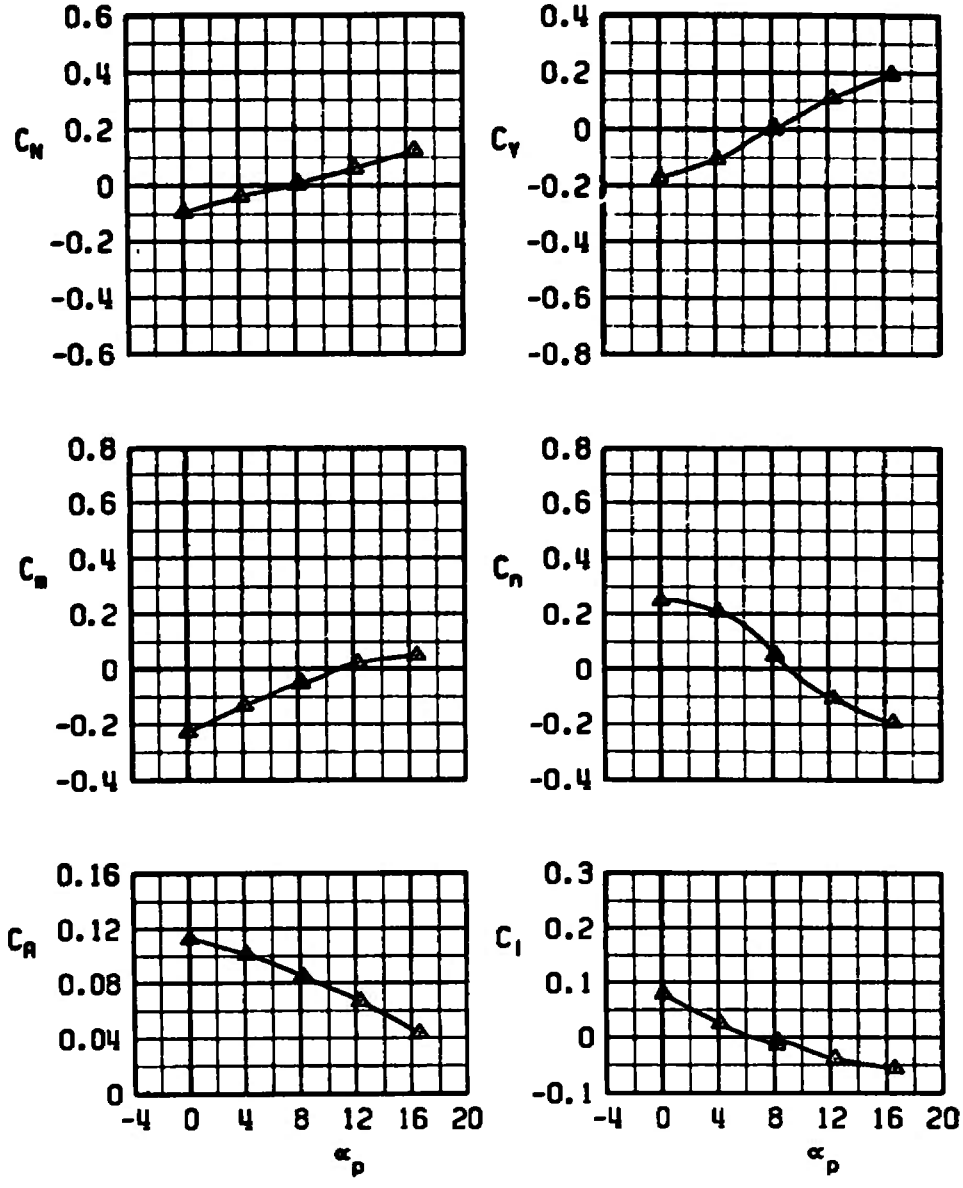

b. Variation with α_p, RW inboard, β_p = 4 deg
Figure 13. Continued.

SYMBOL	M_∞	ϕ_T	β_p	CONFIG	PYLON
⊙	0.7	0	9	3	LW INBD
⊡	0.9	0	9	3	LW INBD
▲	1.3	0	9	3	LW INBD

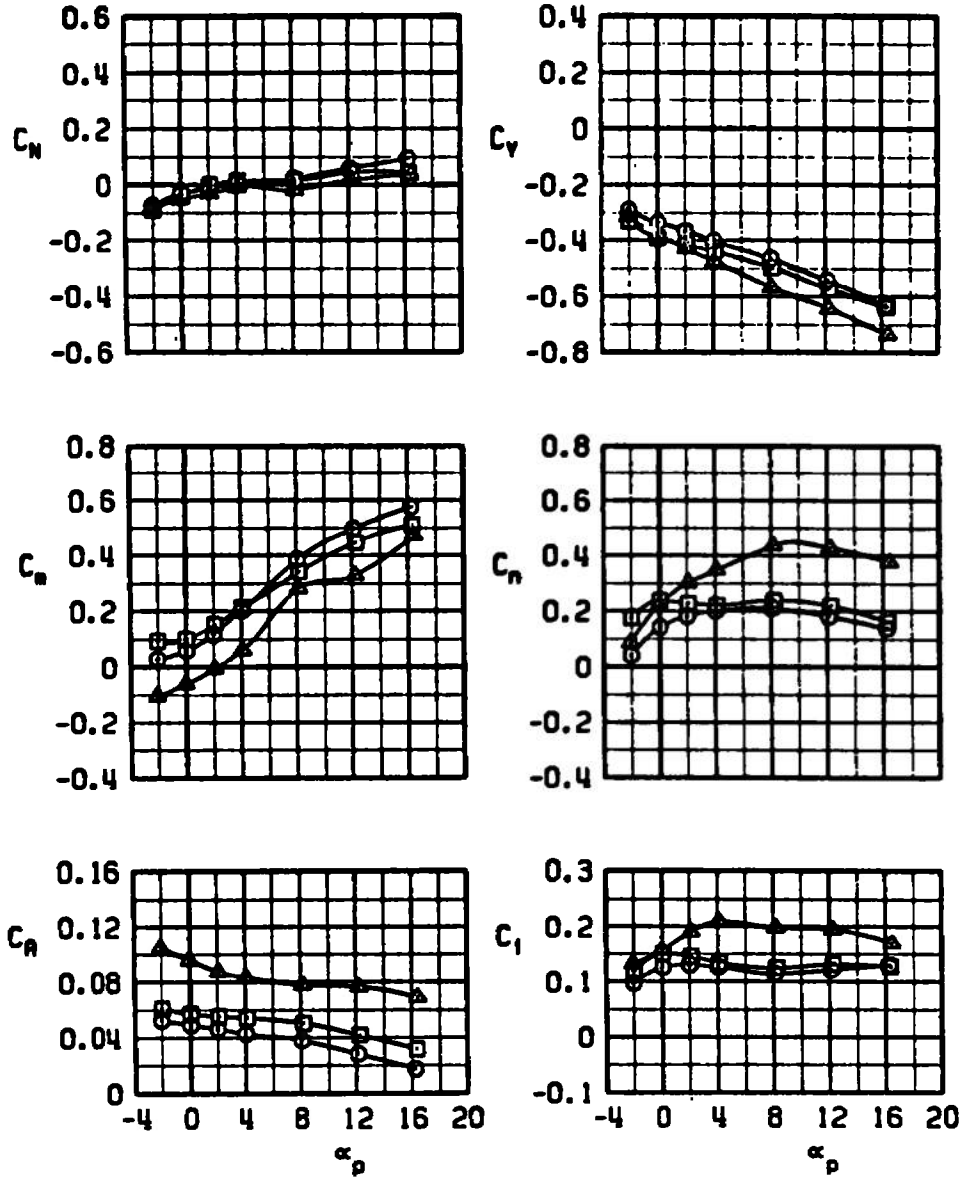

c. Variation with α_p, LW inboard, β_p = 9 deg
Figure 13. Continued.

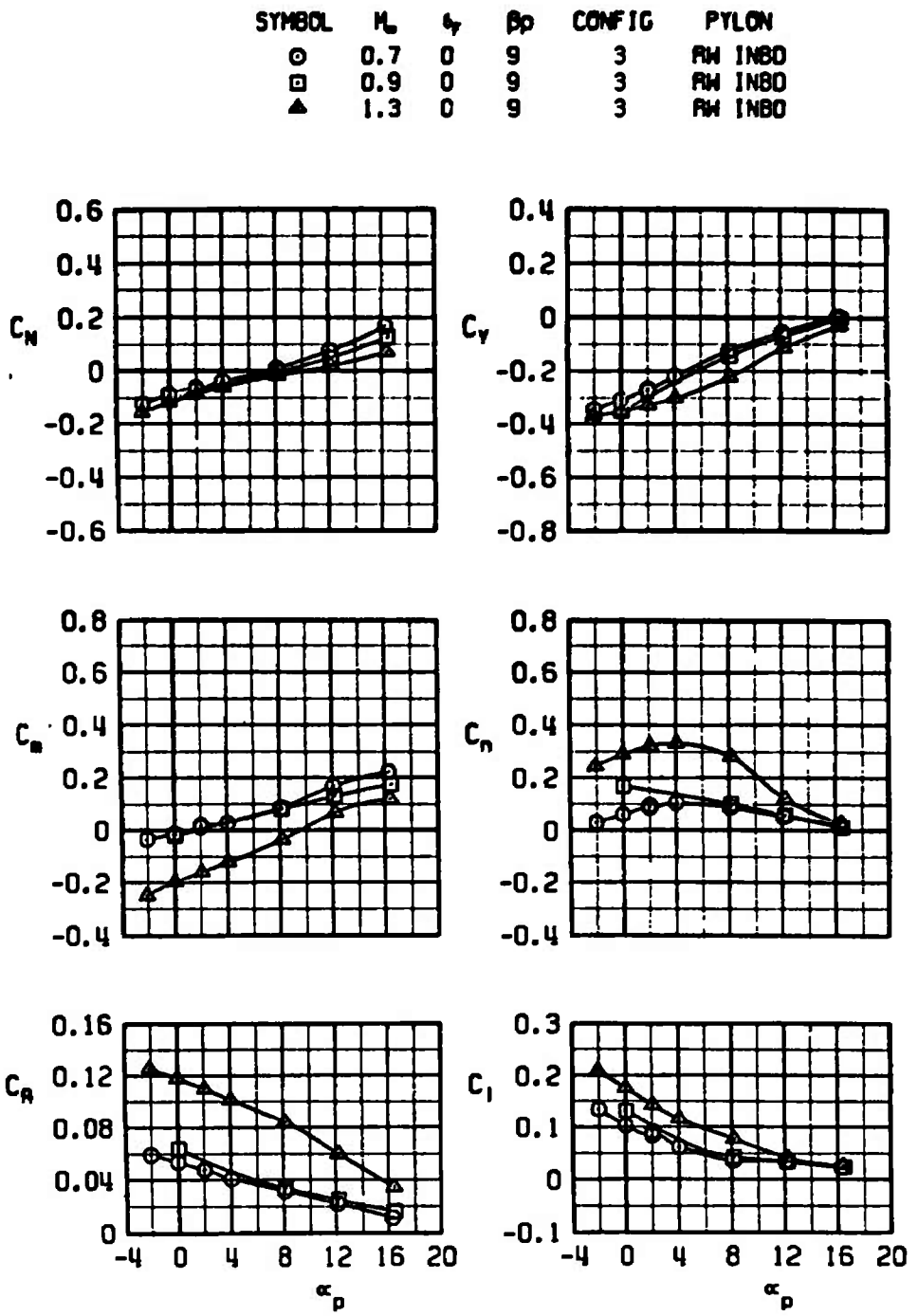

d. Variation with α_p, RW inboard, β_p = 9 deg
Figure 13. Continued.

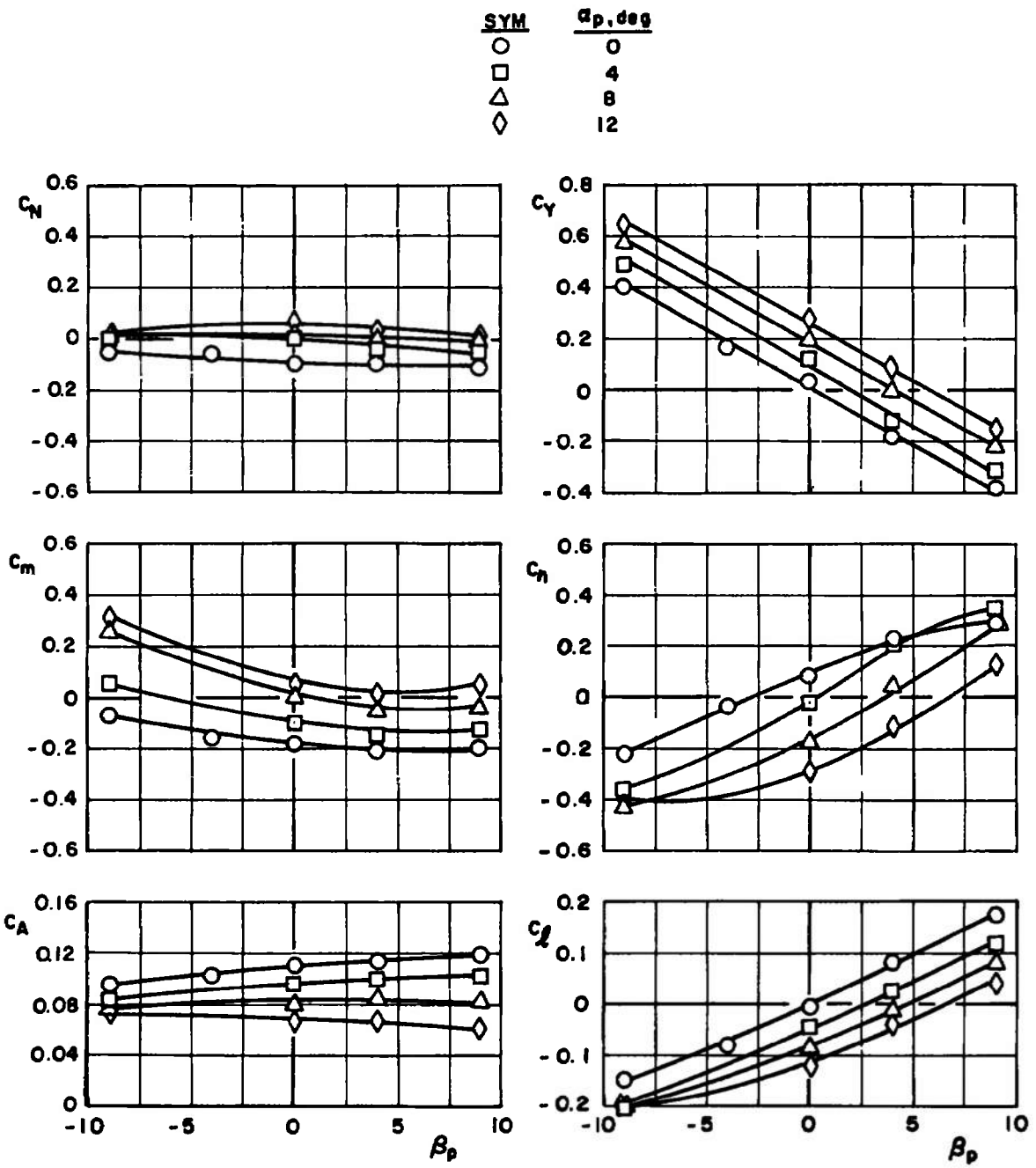

e. Variation with β_p, M_∞ = 1.3, RW inboard
Figure 13. Concluded.

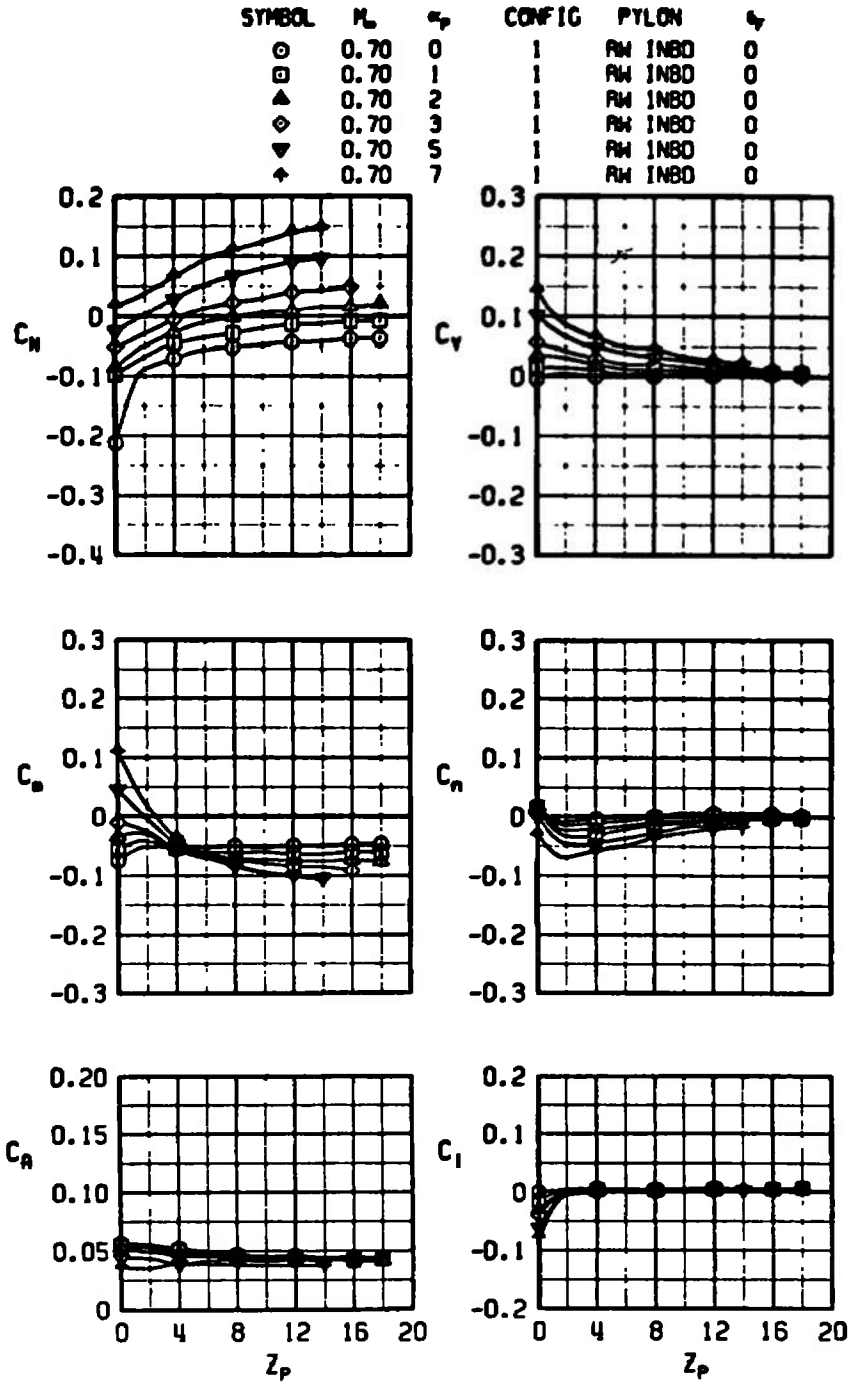

a. $M_\infty = 0.70$, configuration 1

Figure 14. Aerodynamic characteristics of the MGGB MK-II store in the F-4C flow field, $\delta_F = 0$, $X_p = Y_p = 0$, $\beta_p = 0$.

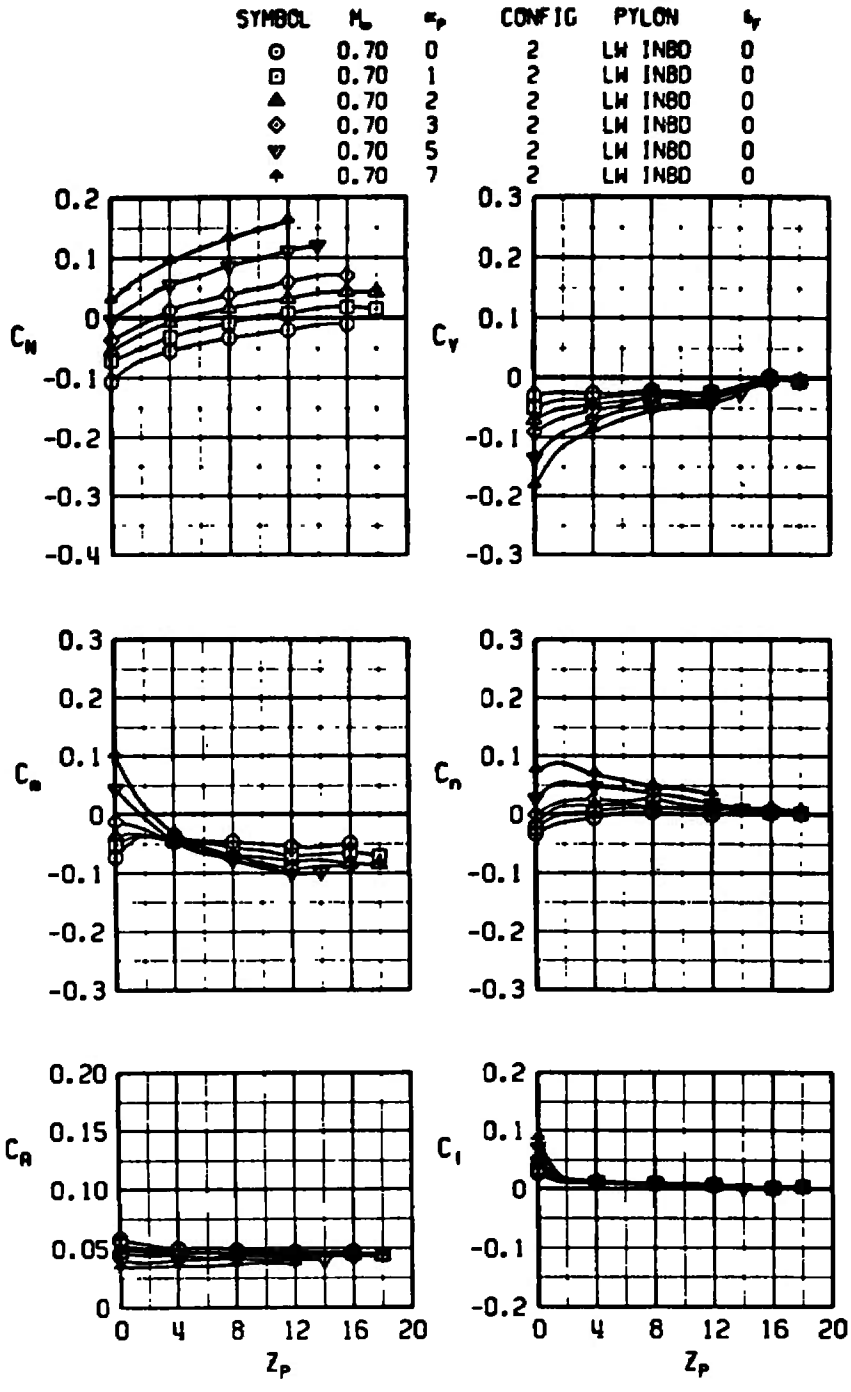

b. M_∞ = 0.70, configuration 2
Figure 14. Continued.

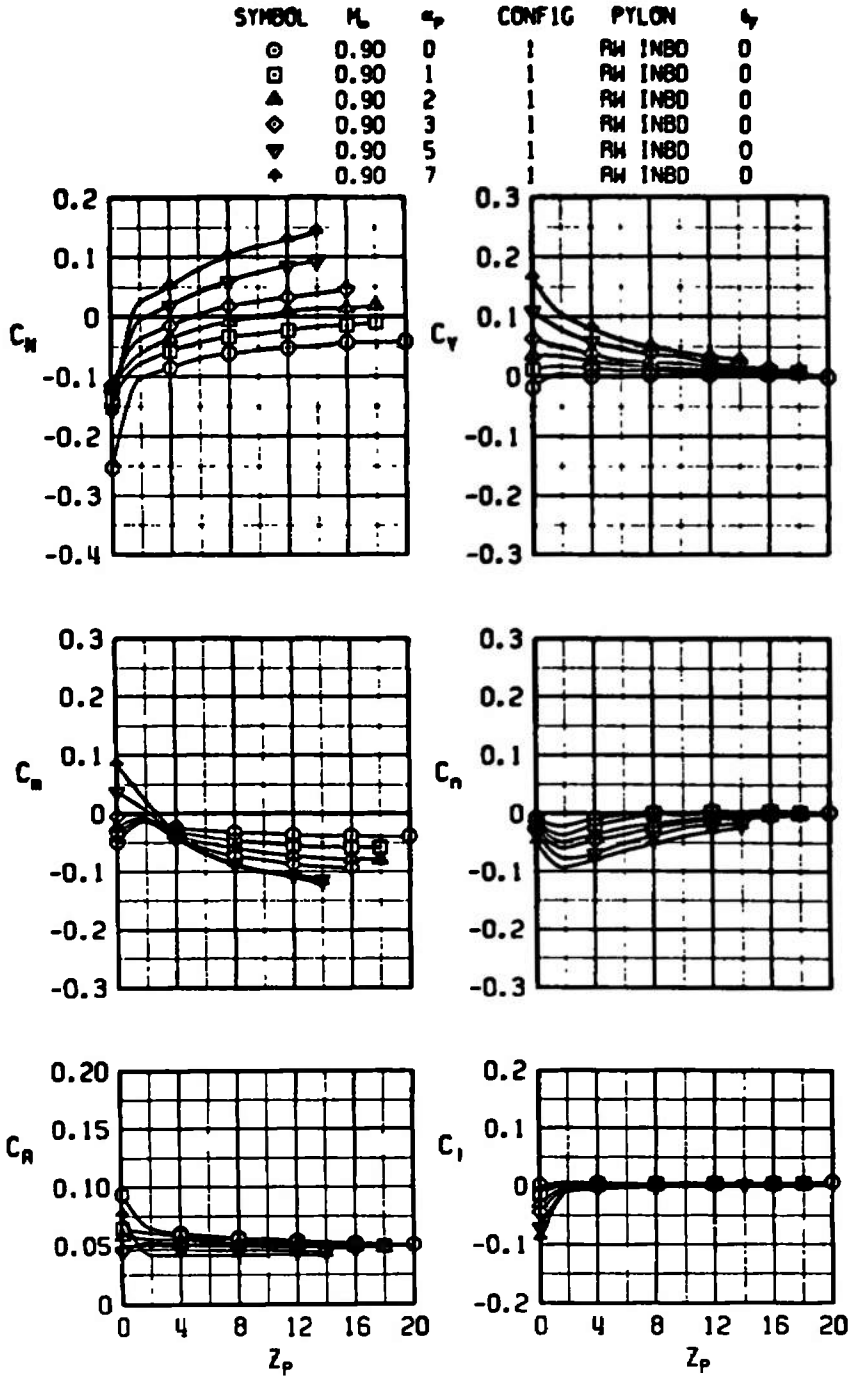

c. M_∞ = 0.90, configuration 1
Figure 14. Continued.

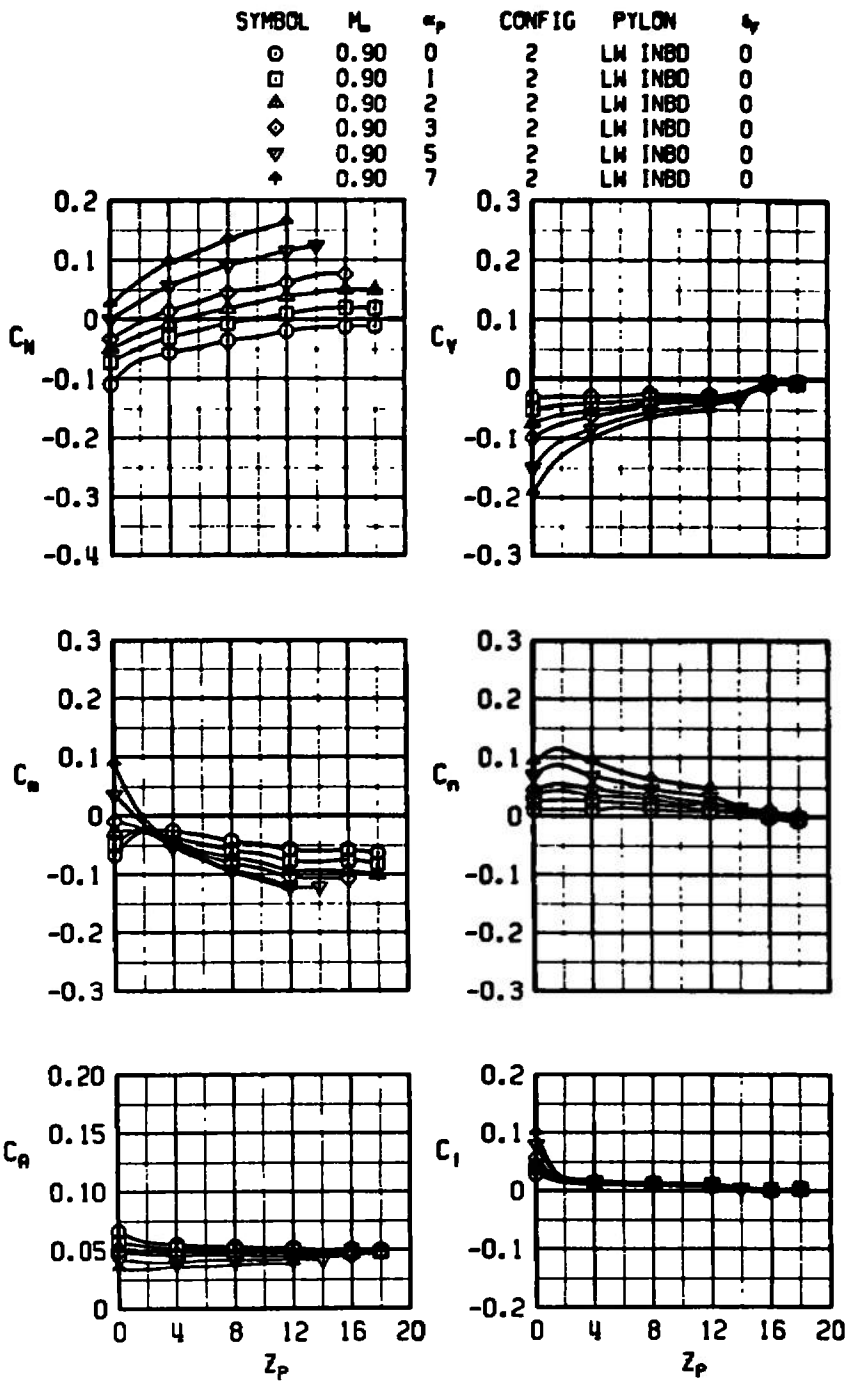

d. M_∞ = 0.90, configuration 2
Figure 14. Continued.

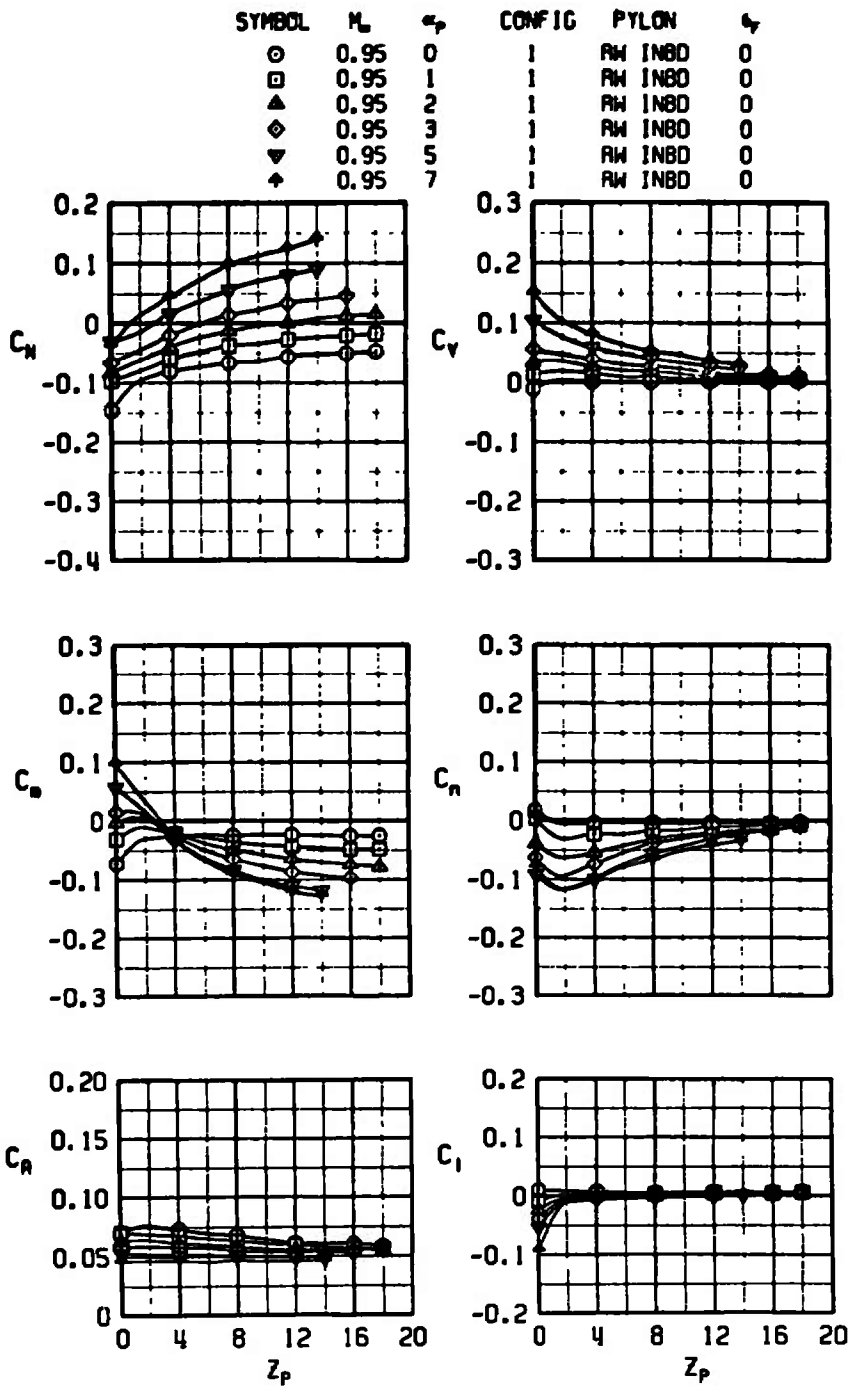

e. M_∞ = 0.95, configuration 1
Figure 14. Continued.

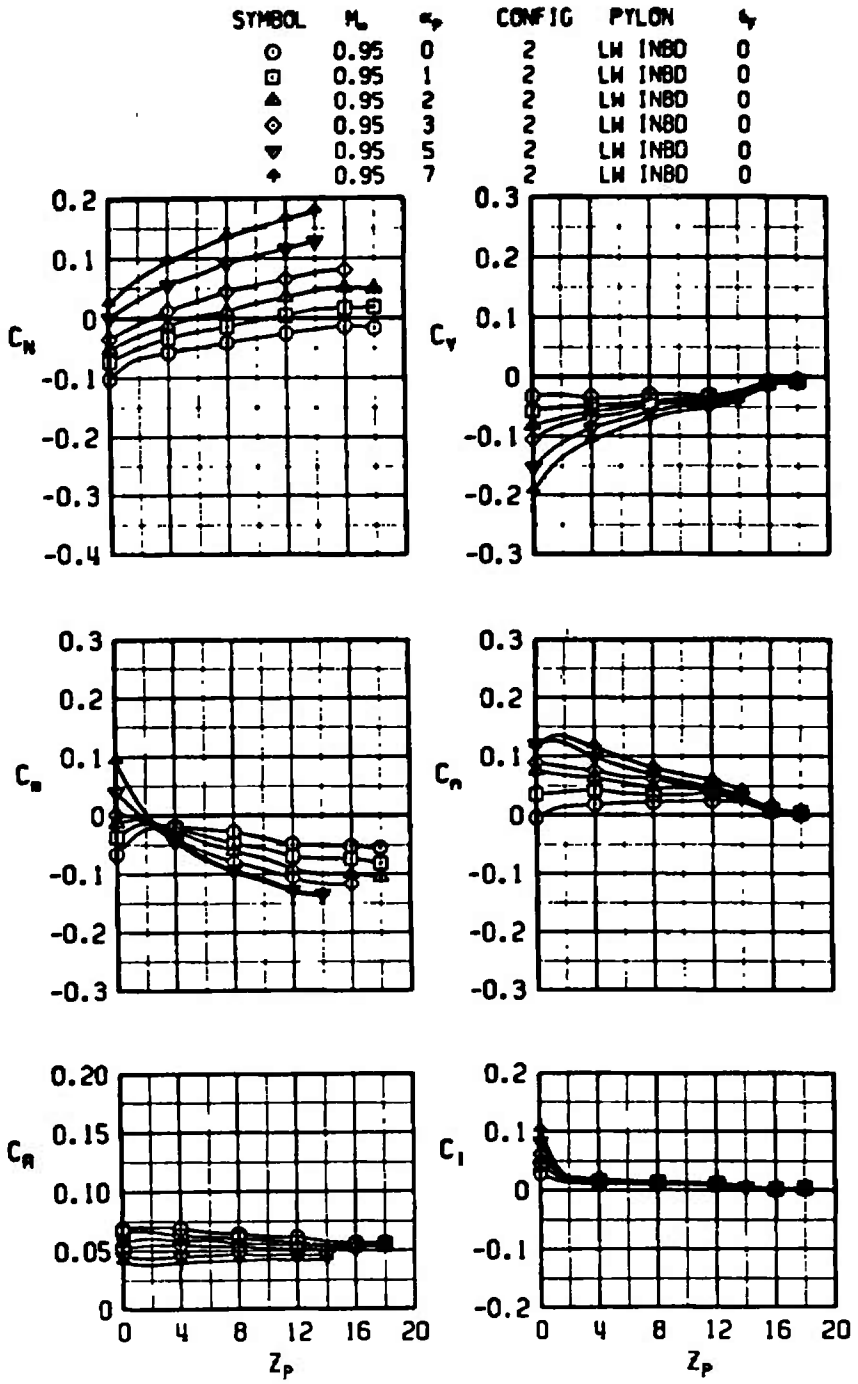

f. M_∞ = 0.95, configuration 2
Figure 14. Continued.

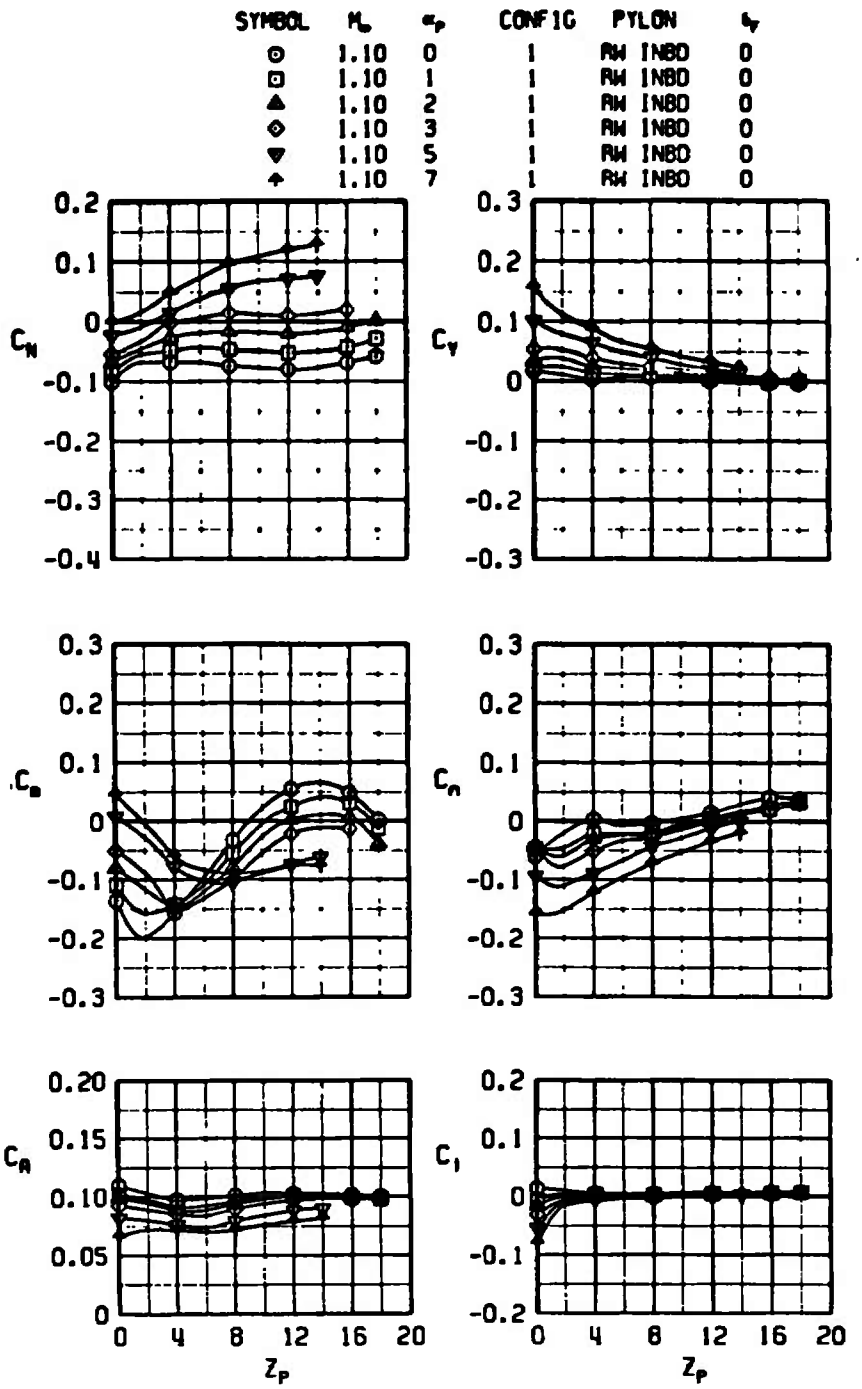

g. M_∞ = 1.10, configuration 1
Figure 14. Continued.

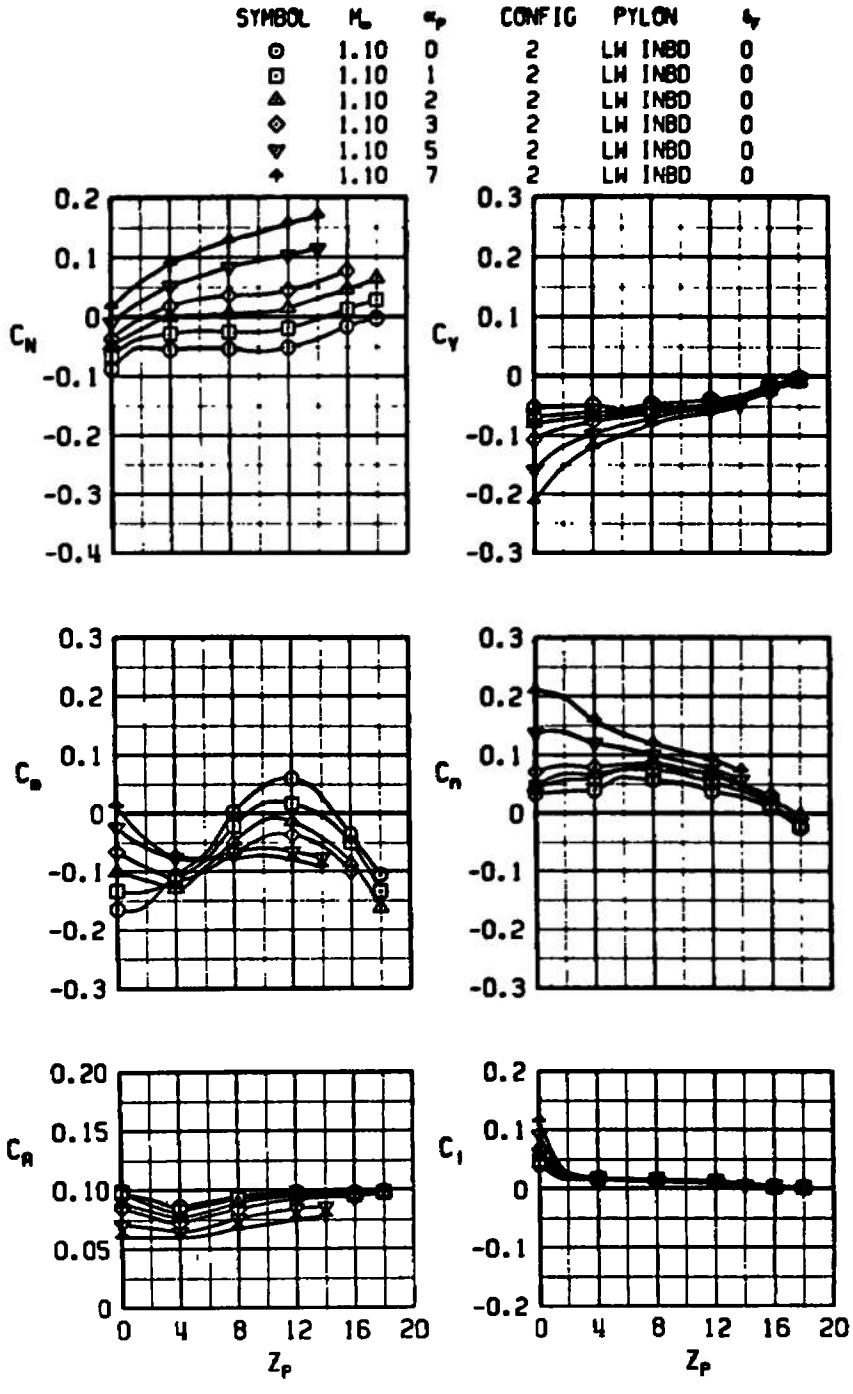

h. M_∞ = 1.10, configuration 2
Figure 14. Continued.

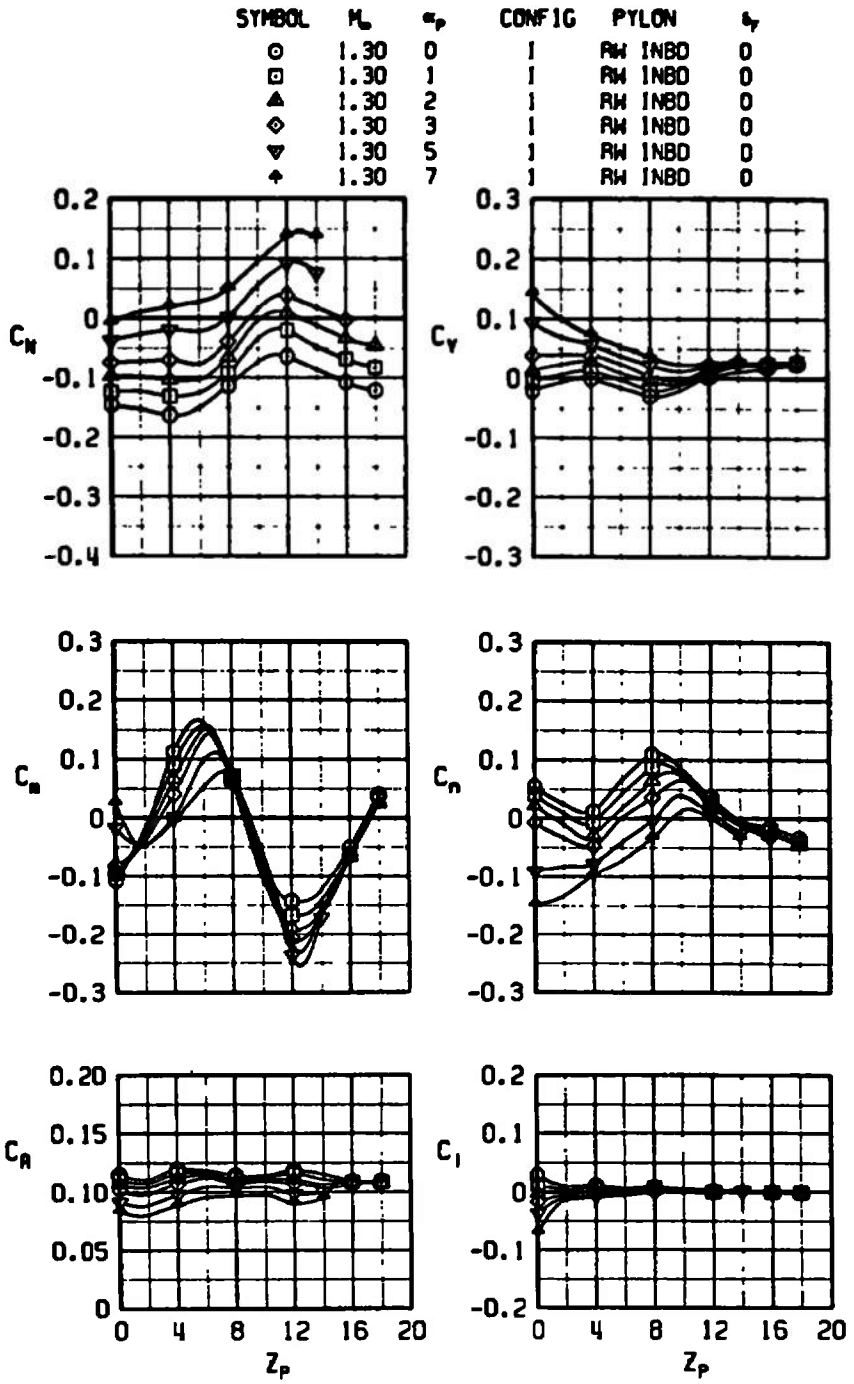

i. M_∞ = 1.30, configuration 1

Figure 14. Continued.

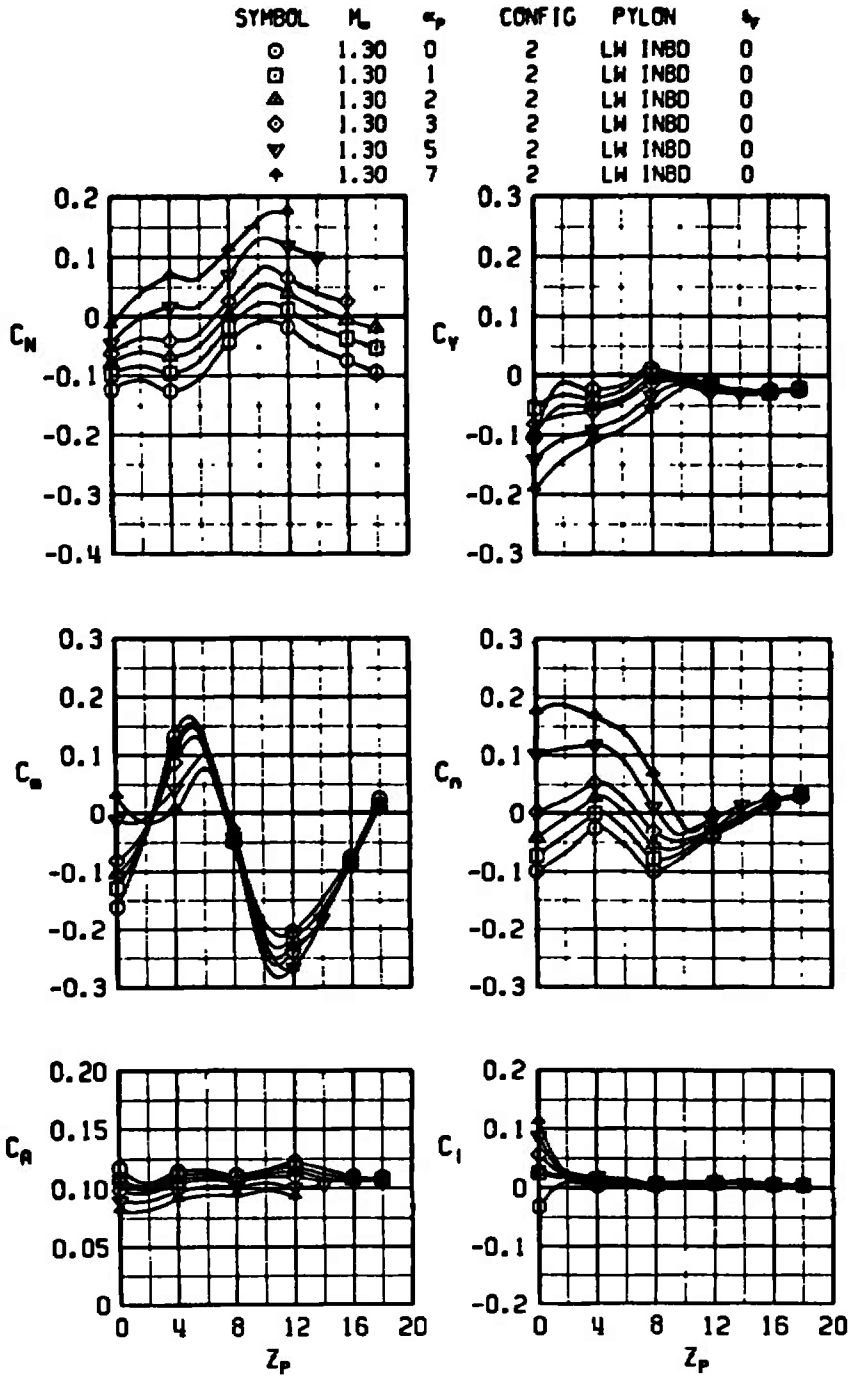

j. M_∞ = 1.30, configuration 2

Figure 14. Concluded.

SYMBOL	M_∞	α_p	CONFIG	PYLON	H	ϕ_p
⊙	0.70	1.5	1	RW INBD	5000	0
⊡	0.70	1.5	1	RW INBD	5000	20
▲	0.70	1.5	1	RW INBD	5000	-20

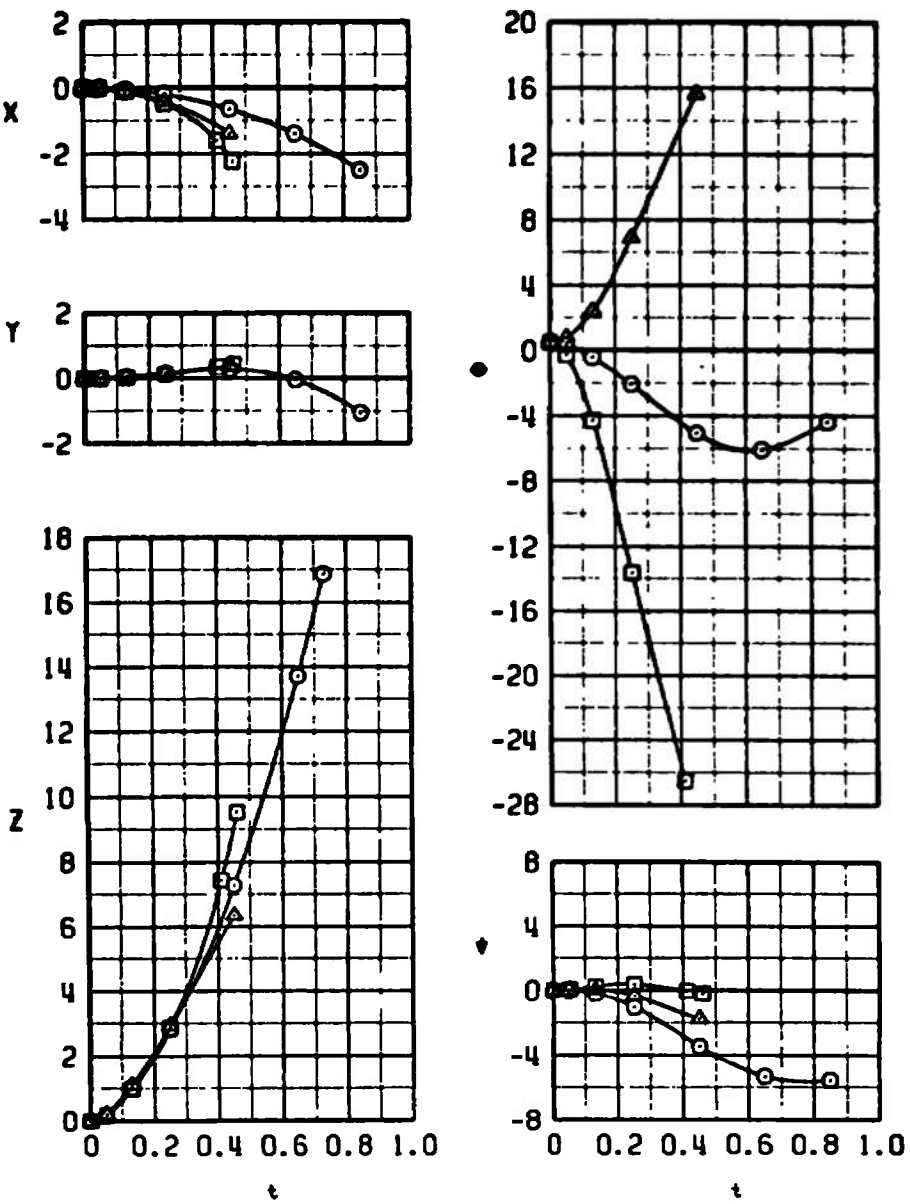

a. M_∞ = 0.70, configuration 1, H = 5,000 ft

Figure 15. Comparison of the MGGB MK-II launch trajectories for different fin deflection angles, β_p = 0.

SYMBOL	M_∞	α_p	CONFIG	PYLON	H	ϕ_T
⊙	0.70	1.5	2	LW INBD	5000	0
⊡	0.70	1.5	2	LW INBD	5000	20
▲	0.70	1.5	2	LW INBD	5000	-20

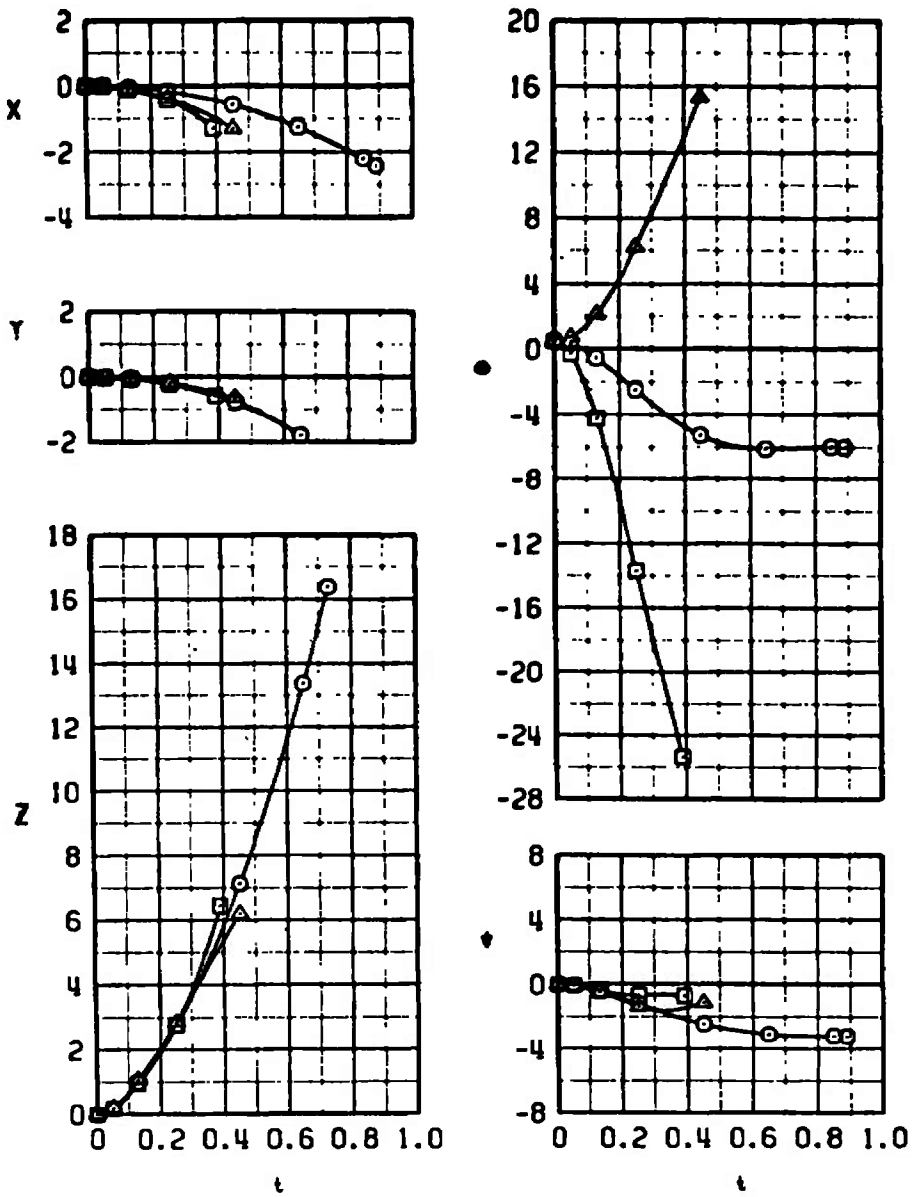

b. M_∞ = 0.70, configuration 2, H = 5,000 ft
Figure 15. Continued.

SYMBOL	M_∞	α_p	CONFIG	PYLON	H	ϕ_p
⊡	0.90	5	1	RW INBD	40000	20
△	0.90	5	1	RW INBD	40000	-20

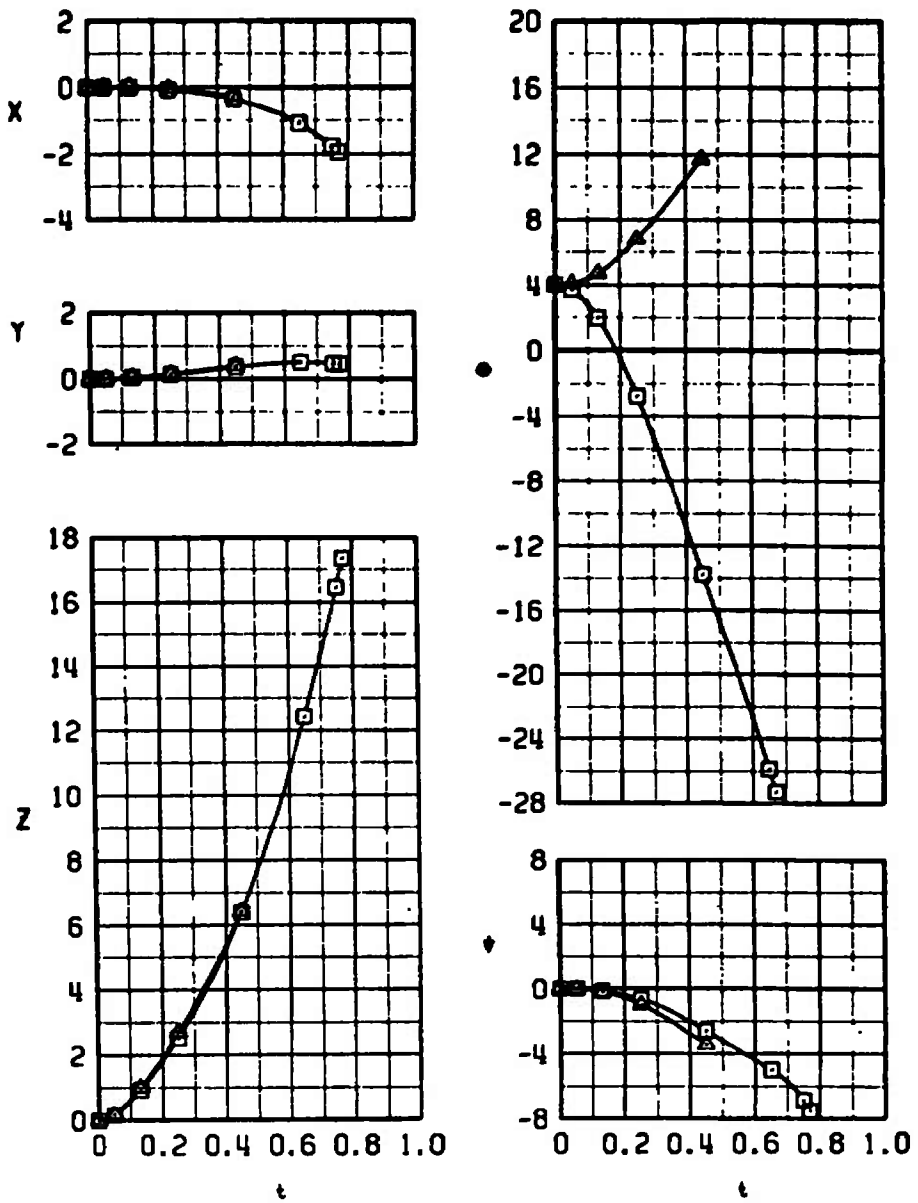

c. M_∞ = 0.90, configuration 1, H = 40,000 ft
Figure 15. Continued.

SYMBOL	M_∞	α_p	CONFIG	PYLON	H	ϕ_r
⊙	0.90	5	2	LW INBD	40000	0
⊡	0.90	5	2	LW INBD	40000	20
△	0.90	5	2	LW INBD	40000	-20

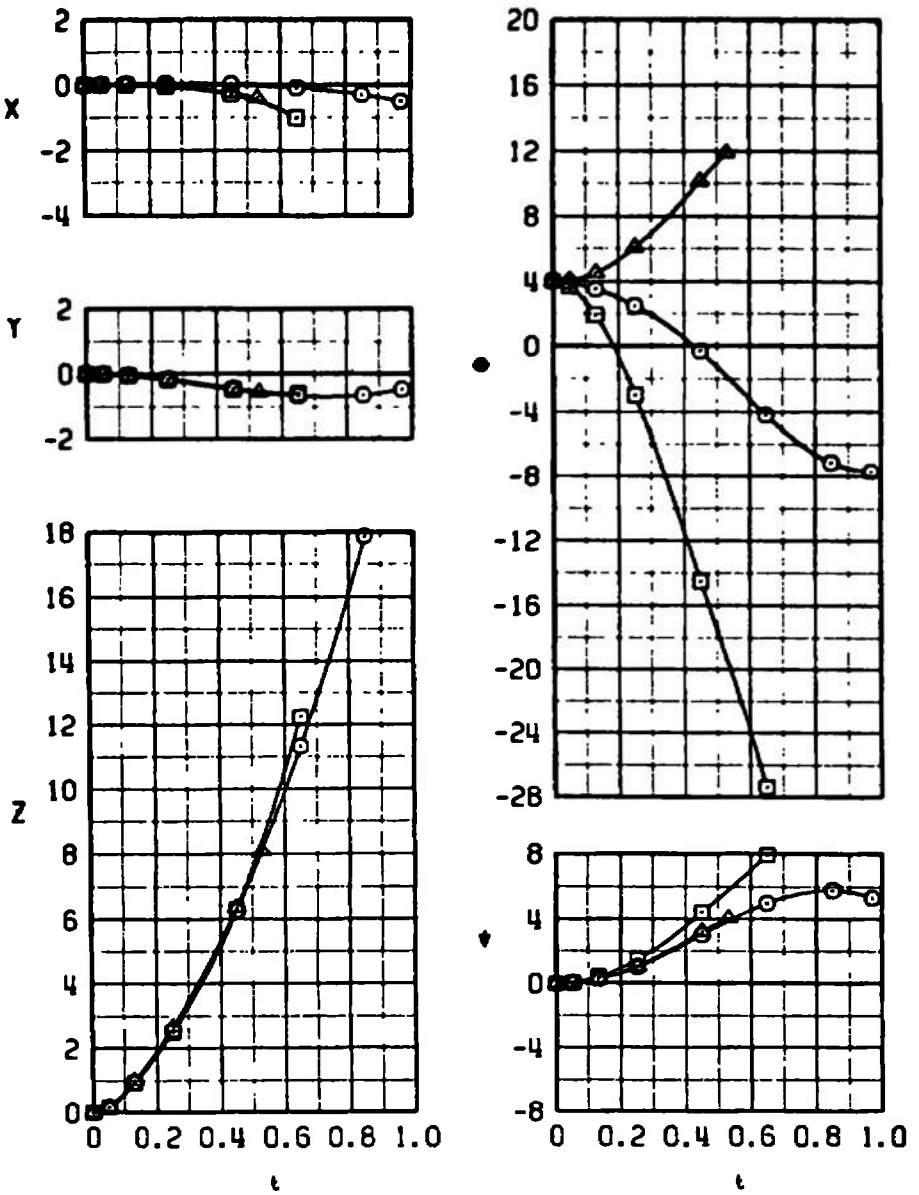

d. M_∞ = 0.90, configuration 2, H = 40,000 ft
Figure 15. Continued.

SYMBOL	M_∞	α_p	CONFIG	PYLON	H	ϕ_T
⊙	0.95	0	1	RW INBD	5000	0
⊡	0.95	0	1	RW INBD	5000	20
△	0.95	0	1	RW INBD	5000	-20

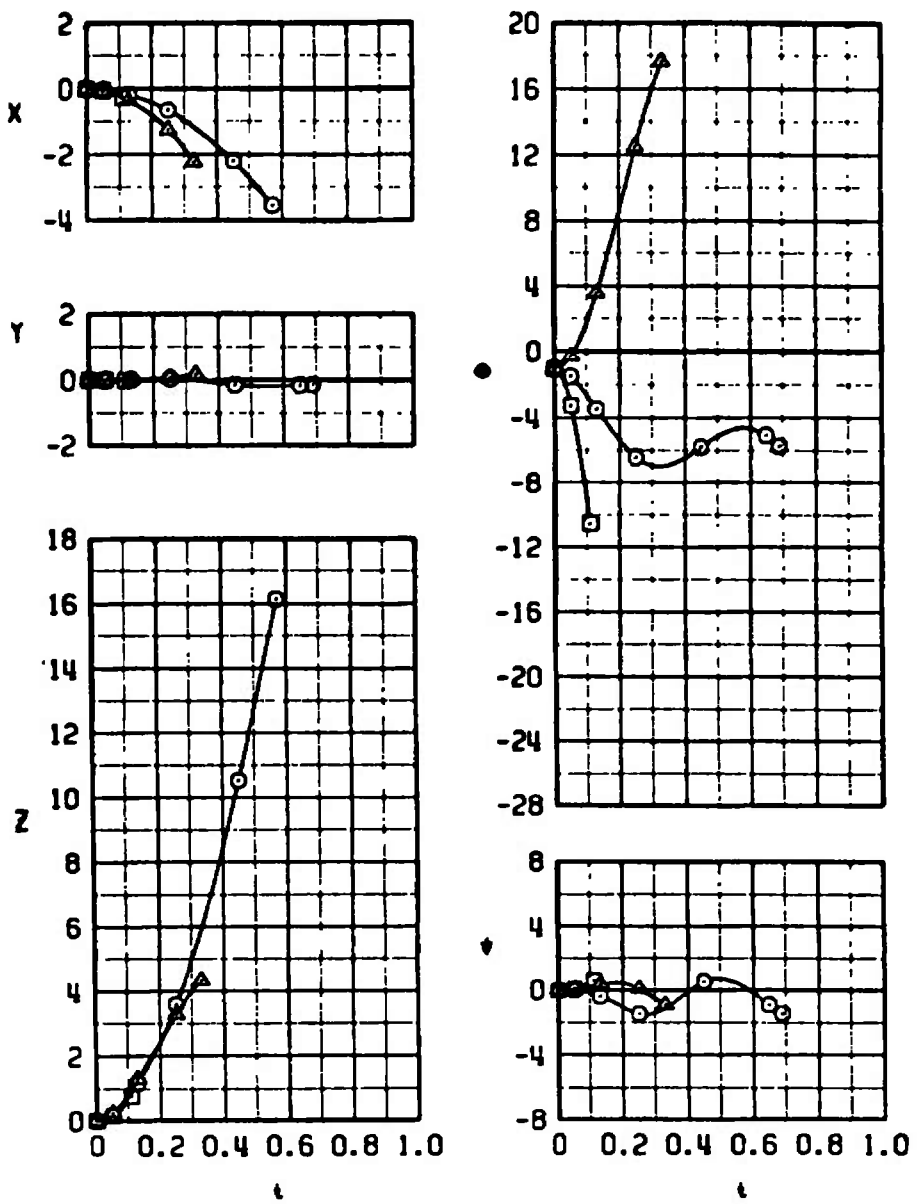

e. M_∞ = 0.95, configuration 1, H = 5,000 ft
Figure 15. Continued.

SYMBOL	M_∞	α_p	CONFIG	PYLON	H	ϕ_v
⊙	0.95	0	2	LW INBD	5000	0
⊡	0.95	0	2	LW INBD	5000	20
▲	0.95	0	2	LW INBD	5000	-20

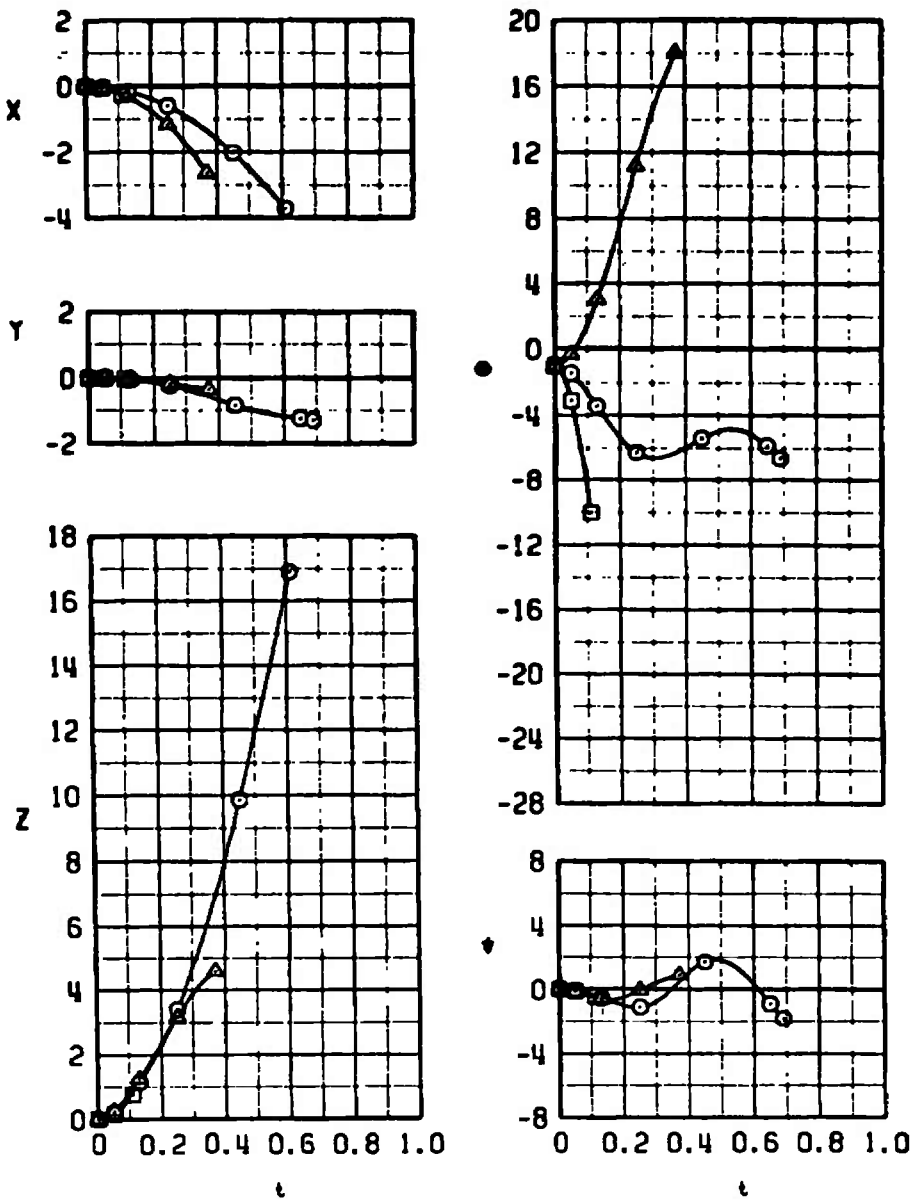

f. M_∞ = 0.95, configuration 2, H = 5,000 ft
Figure 15. Continued.

SYMBOL	M_∞	α_p	CONFIG	PYLON	H	ϕ_p
⊙	0.95	3.5	1	RW INBD	40000	0
⊡	0.95	3.5	1	RW INBD	40000	20
△	0.95	3.5	1	RW INBD	40000	-20

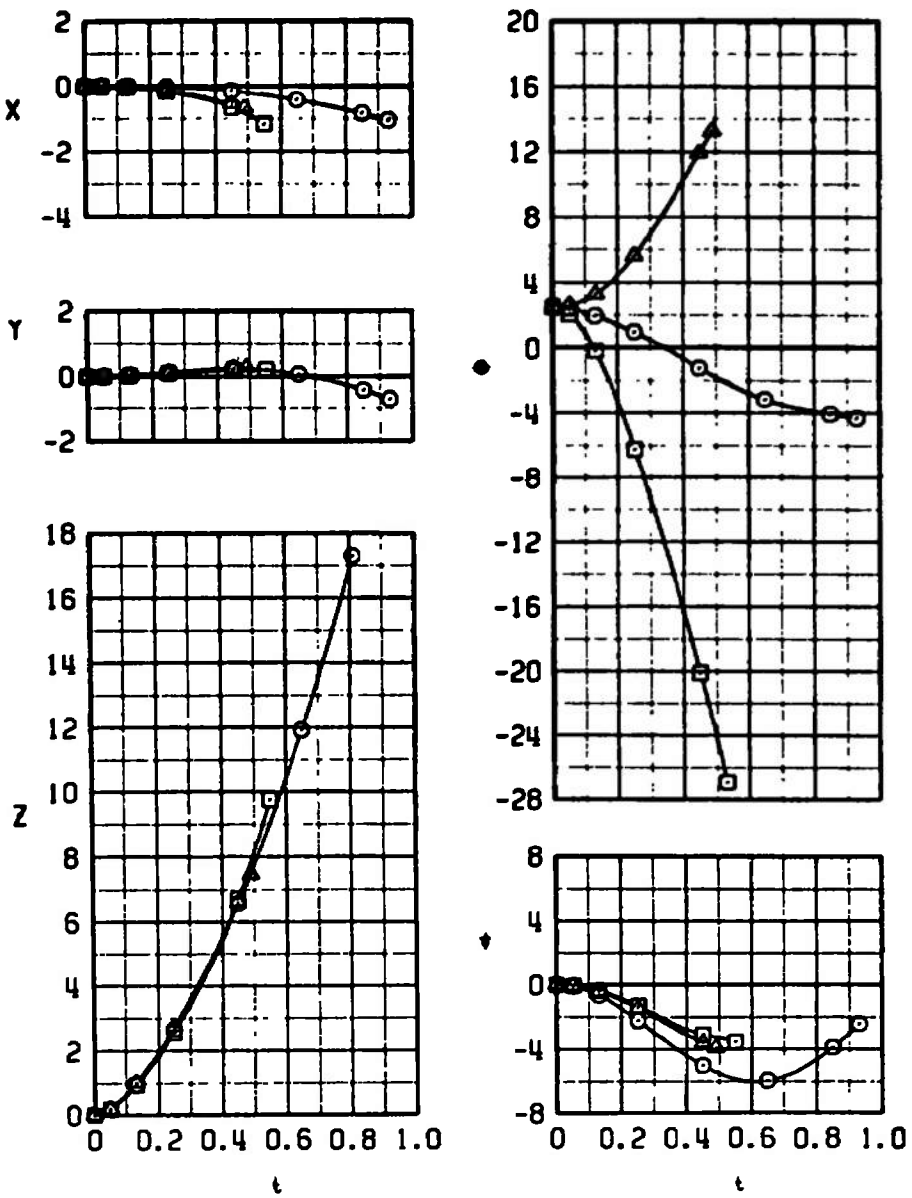

g. M_∞ = 0.95, configuration 1, H = 40,000 ft
Figure 15. Continued.

SYMBOL	M_∞	α_p	CONFIG	PYLON	H	ϕ_p
⊡	0.95	3.5	2	LW INBD	40000	20
⊙	0.95	3.5	2	LW INBD	40000	0
△	0.95	3.5	2	LW INBD	40000	-20

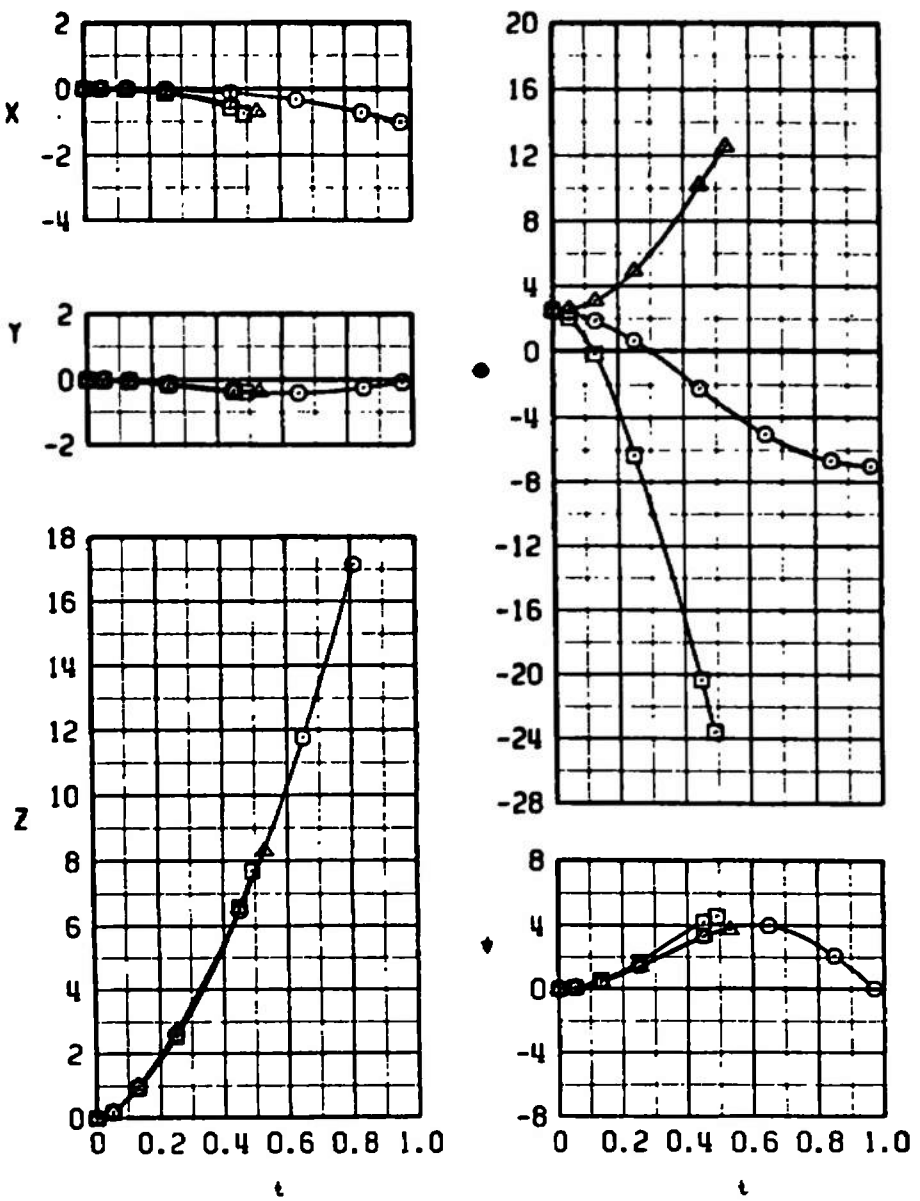

h. M_∞ = 0.95, configuration 2, H = 40,000 ft
Figure 15. Continued.

SYMBOL	M_∞	α_p	CONFIG	PYLON	H	ϕ_p
⊙	1.30	2.5	1	RW INBD	40000	0
⊡	1.30	2.5	1	RW INBD	40000	20
△	1.30	2.5	1	RW INBD	40000	-20

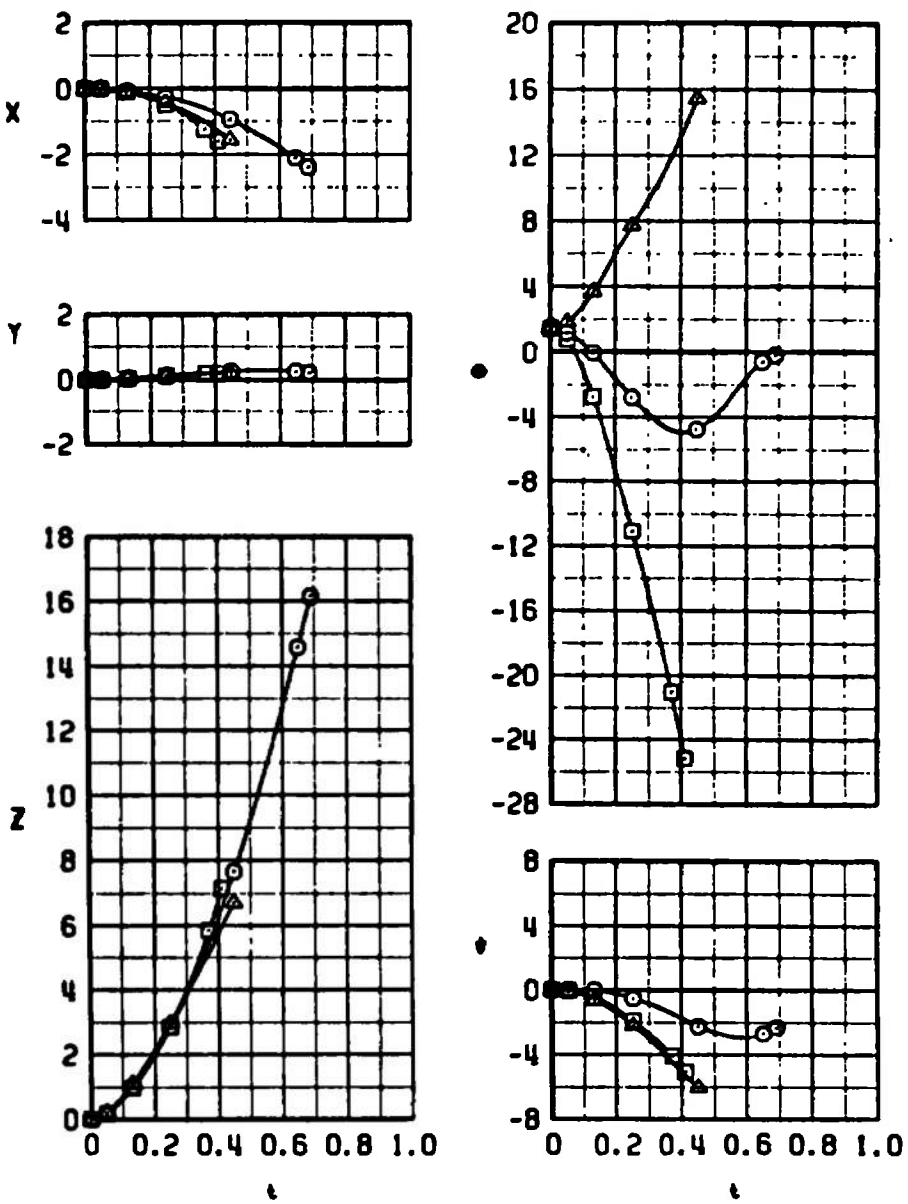

i. M_∞ = 1.30, configuration 1, H = 40,000 ft
Figure 15. Continued.

SYMBOL	M_∞	α_p	CONFIG	PYLON	H	ϕ_T
⊙	1.30	2.5	2	LW INBD	40000	0
⊡	1.30	2.5	2	LW INBD	40000	20
▲	1.30	2.5	2	LW INBD	40000	-20

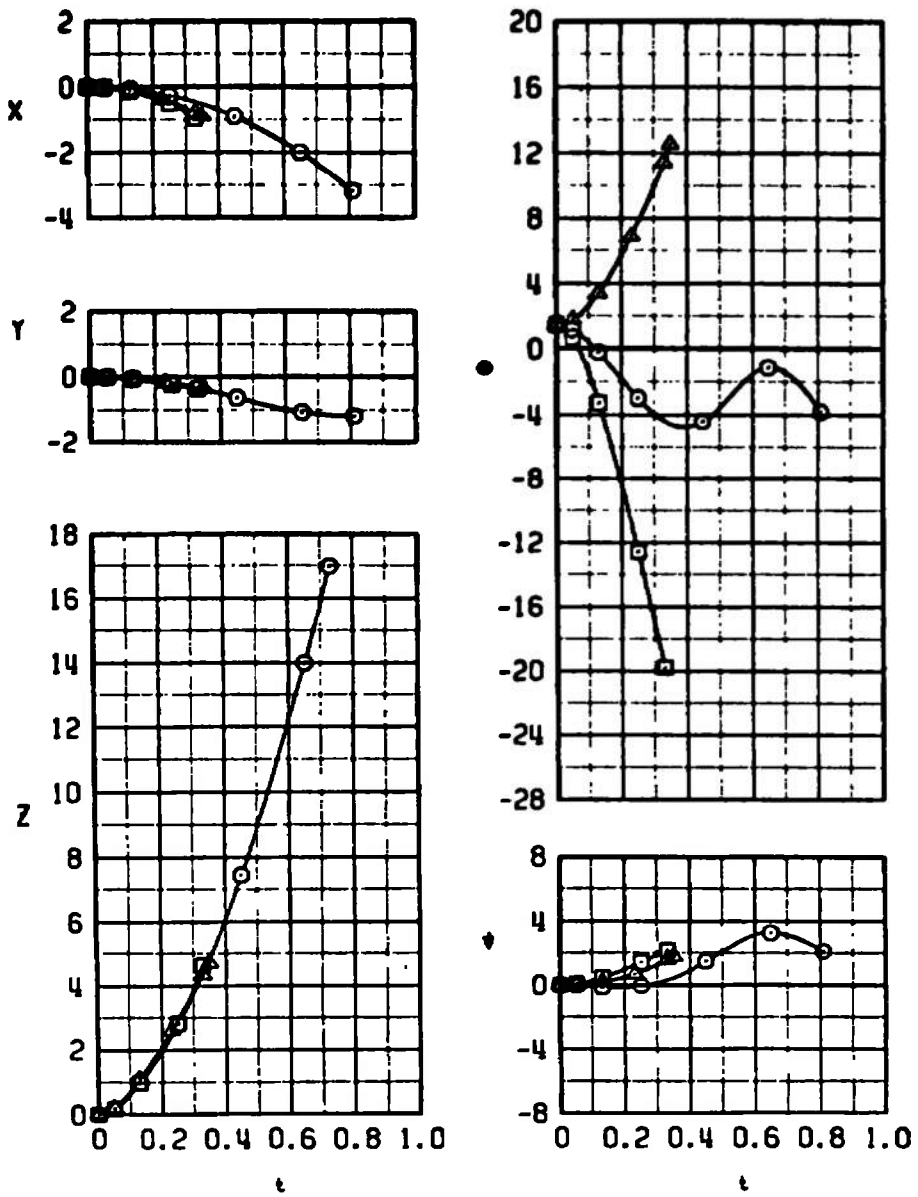

j. M_∞ = 1.30, configuration 2, H = 40,000 ft
Figure 15. Concluded.

Table 1. Wind Tunnel Test Conditions

M_∞	p_t, psfa	T_t, °R	q_∞, psf	p_∞, psfa	$Re_\infty \times 10^{-6}$, ft^{-1}
0.70	1200	560	300	870	2.1
0.90	↓	↓	400	710	2.4
0.95			420	670	2.4
1.10			480	560	2.5
1.30			510	430	2.5

Table 2. Test Summary

δ_F	α_B	β_W	M_∞					Type Data
			0.7	0.9	0.95	1.1	1.3	
0, 20, -20	-20 to 20	0	x	x	x	x	x	Free-Stream Aerodynamic
0	0, 5, -5	-20 to 20	x	x	x	x	x	Free-Stream Aerodynamic

Config-uration	α_P	β_P	Z_P	δ_F	M_∞					Type Data
					0.7	0.9	0.95	1.1	1.3	
3	-2 to 16	0,±9	0	0	x	x			x	Flow-Field Aerodynamic
3	-2 to 16	±4	0	↓					x	↓
1, 2	0,1,2,3, 5,7	0	0 to 20	↓	x	x	x	x	x	↓

Config-uration	δ_F	H	α_P	β_P	M_∞					Type Data
					0.7	0.9	0.95	1.1	1.3	
1, 2	0,20,-20	5K	0	0			x			Separation Trajectory
↓	↓	5K	1.5	↓	x		↓			↓
		40K	2.5						x	
		↓	3.5				x			
↓	↓	↓	5	↓		x				↓

Table 3. Full-Scale Store Parameters Used in Trajectory Calculations

Symbol	Parameter	Value
S	Store Reference Area, ft^2	16.59
b	Store Reference Width, ft	1.54
I_{xx}	Moment of Inertia, slug-ft^2	45
I_{yy}	Moment of Inertia, slug-ft^2	612
I_{zz}	Moment of Inertia, slug-ft^2	602
C_{m_q}	Pitch-Damping Derivative, per rad	-25
C_{n_r}	Yaw-Damping Derivative, per rad	-25
X_{cg}	Center-of-Gravity Location from Nose, ft	7.16
Z_{cg}	Center-of-Gravity Location above Centerline, ft	0.142
$\bar{m}$	Mass, slugs	82.34
γ	Dive Angle, deg	0
F_{Z_1}	Forward Ejector Force, lb	4075
F_{Z_2}	Aft Ejector Force, lb	4075
X_{L_1}	Forward Ejector Piston Location, ft	0.908
X_{L_2}	Aft Ejector Piston Location, ft	-0.759
Z_E	Ejector Stroke Length, ft	0.375

Table 4. Adjustments to Pitching-Moment Coefficients for Trajectory Calculations

Symbol	Parameter	Value at M_∞				
		0.70	0.90	0.95	1.10	1.30
C_{m_o}	Pitching-Moment Coefficient Correction	-0.026	-0.060	-0.070	-0.035	-0.040
ΔX_{cg}	Pitching-Moment Slope Coefficient Correction, in.	0.101	0.128	0.024	0	0

NOMENCLATURE

BL	Aircraft buttock line from plane of symmetry, in., model scale
b	Store reference dimension, ft, full scale
C_A	Store measured axial-force coefficient, axial force/$q_\infty S$
C_ℓ	Store rolling-moment coefficient, rolling moment/$q_\infty Sb$
C_{ℓ_β}	Store rolling-moment coefficient derivative, $\partial C_\ell / \partial \beta_W$, per deg
C_m	Store pitching-moment coefficient, referenced to the store cg, pitching moment/$q_\infty Sb$
C_{m_o}	Store pitching-moment coefficient correction, difference in measured pitching-moment coefficients for 0.20-scale and 0.05-scale models at $\alpha_B = 0$
C_{m_q}	Store pitch-damping derivative, $dC_m/d(qb/2V_\infty)$
C_{m_α}	Store pitching-moment coefficient derivative, $\partial C_m / \partial \alpha_B$, per deg
C_N	Store normal-force coefficient, normal force/$q_\infty S$
C_{N_α}	Store normal-force coefficient derivative, $\partial C_N / \partial \alpha_B$, per deg
C_n	Store yawing-moment coefficient, referenced to the store cg, yawing moment/$q_\infty Sb$
C_{n_r}	Store yaw-damping derivative, $dC_n/d(rb/2V_\infty)$
C_{n_β}	Store yawing-moment coefficient derivative, $\partial C_n / \partial \beta_W$, per deg
C_Y	Store side-force coefficient, side force/$q_\infty S$
C_{Y_β}	Store side-force coefficient derivative, $\partial C_Y / \partial \beta_W$, per deg
FS	Aircraft fuselage station, in., model scale
F_{Z_1}	Forward ejector force, lb
F_{Z_2}	Aft ejector force, lb
H	Pressure altitude, ft

I_{xx} Full-scale moment of inertia about the store X_B axis, slug-ft^2

I_{yy} Full-scale moment of inertia about the store Y_B axis, slug-ft^2

I_{zz} Full-scale moment of inertia about the store Z_B axis, slug-ft^2

M_∞ Free-stream Mach number

$\overline{m}$ Full-scale store mass, slugs

p_t Free-stream total pressure, psfa

p_∞ Free-stream static pressure, psfa

q Store angular velocity about the Y_B axis, radians/sec

q_∞ Free-stream dynamic pressure, psf

Re_∞ Free-stream unit Reynolds number, per ft

r Store angular velocity about the Z_B axis, radians/sec

S Store reference area, ft^2, full scale

T_t Free-stream total temperature, °R

t Real trajectory time from initiation of trajectory, sec

V_∞ Free-stream velocity, ft/sec

WL Aircraft waterline from reference horizontal plane, in., model scale

X Separation distance of the store cg parallel to the flight axis system X_F direction, ft, full scale measured from the prelaunch position

X_{cg} Full-scale cg location, ft, from nose of store

ΔX_{cg} Store moment reference correction factor, in., model scale, positive for forward movement

X_{L_1} Forward ejector location relative to the store cg, positive forward of store cg, ft, full scale

X_{L_2} Aft ejector piston location relative to the store cg, positive forward of store cg, ft, full scale

Y Separation distance of the store cg parallel to the flight axis system Y_F direction, ft, full scale measured from the prelaunch position

Z Separation distance of the store cg parallel to the flight-axis system Z_F direction, ft, full scale measured from the prelaunch position

Z_{cg} Full-scale cg location, ft, above centerline of store

Z_E Ejector stroke, ft

α_B Store model angle of attack relative to the free-stream velocity vector, deg

α_P Parent-aircraft model angle of attack relative to the free-stream velocity vector, deg

β_P Parent-aircraft model sideslip angle relative to the free-stream velocity vector, deg

β_W Store model sideslip angle relative to the free-stream velocity vector, deg

δ_F Store fin deflection angle, deg (see Fig. 6)

θ Angle between the store longitudinal axis and its projection in the X_F-Y_F plane, positive when store nose is raised as seen by the pilot, deg

γ Simulated parent-aircraft dive angle, angle between the flight direction and the earth horizontal, deg, positive for decreasing altitude

ψ Angle between the projection of the store longitudinal axis in the X_F-Y_F plane and the X_F axis, positive when the store nose is to the right as seen by the pilot, deg

FLIGHT-AXIS SYSTEM COORDINATES

Directions

X_F Parallel to the free-stream wind vector, positive direction is forward as seen by the pilot

Y_F Perpendicular to the X_F and Z_F directions, positive direction is to the right as seen by the pilot

Z_F In the aircraft plane of symmetry, perpendicular to the free-stream wind vector, positive direction is downward

The flight-axis system origin is coincident with the aircraft cg and remains fixed with respect to the parent aircraft during store separation. The X_F, Y_F, and Z_F coordinate axes do not rotate with respect to the initial flight direction and attitude.

STORE BODY-AXIS SYSTEM COORDINATES

Directions

X_B Parallel to the store longitudinal axis, positive direction is upstream in the prelaunch position

Y_B Perpendicular to the store longitudinal axis, and parallel to the flight-axis system X_F-Y_F plane when the store is at zero roll angle, positive direction is to the right looking upstream when the store is at zero yaw and roll angles

Z_B Perpendicular to both the X_B and Y_B axes, positive direction is downward as seen by the pilot when the store is at zero pitch and roll angles

The store body-axis system origin is coincident with the store cg and moves with the store during separation from the parent airplane. The X_B, Y_B, and Z_B coordinate axes rotate with the store in pitch, yaw, and roll so that mass moments of inertia about the three axes are not time-varying quantities.

PYLON-AXIS SYSTEM COORDINATES

Directions

X_P Parallel to the store longitudinal axis in the prelaunch carriage position, positive direction is forward as seen by the pilot

Y_P Perpendicular to the X_P axis and parallel to the flight-axis system X_F-Y_F plane, positive direction is to the right as seen by the pilot

Z_P Perpendicular to both the X_P and Y_P axes, positive direction is downward

The pylon-axis system origin is coincident with the store cg in the prelaunch carriage position. The axes are rotated with respect to the flight-axis system by the prelaunch yaw and pitch angles of the store. Both the origin and the direction of the coordinate axes remain fixed with respect to the flight-axis system throughout the trajectory.